Spin conductances and magnetization production in chiral molecular junctions

Richard Korytár,[*],[†] Jan M. van Ruitenbeek,[‡] and Ferdinand Evers[¶]

†*Department of Condensed Matter Physics, Faculty of Mathematics and Physics, Charles University, Ke Karlovu 5, 121 16, Praha 2, Czech Republic*

‡*Huygens-Kamerlingh Onnes Laboratory, Leiden University, NL-2333CA Leiden, Netherlands*

¶*Institute of Theoretical Physics, University of Regensburg, D-93050 Regensburg, Germany*

E-mail: richard.korytar@ur.de

Abstract

Motivated by experimental reports on chirality induced spin selectivity, we investigate a minimal model that allows us to calculate the charge and spin conductances through helical molecules analytically. The spin-orbit interaction is assumed to be non-vanishing on the molecule and negligible in the reservoirs (leads). The band-structure of the molecule features four helical modes with spin-momentum locking that are analogous of edge-currents in the quantum spin Hall effect. While charge is conserved and therefore the charge current is independent of where it is measured, - reservoirs or molecule, - our detailed calculations reveal that the spin currents in the left and right lead are equal in magnitudes but with opposite signs (in linear response). We predict that transport currents flowing through helical molecules are accompanied by a spin accumulation in the contact region with the same magnetization direction for source and drain. Further, we predict that the spin-conductance can be extracted directly

1

from measuring the (quasi-static) spin accumulation - rather than the spin current itself, which is very challenging to obtain experimentally.

Keywords

Chirality-induced spin selectivity, molecular junctions, spintronics

Introduction

Charge currents are routinely measured and analyzed in molecular electronics.[1] The discovery of a family of phenomena that exhibit chirality induced spin selectivity (CISS) has led to a resurge of interest in spin-related phenomena in this field.[2–7] Specifically, experiments report a strong correlation between molecular chirality and a preferred spin direction in systems that exhibit a (nominally) very weak spin-orbit interaction. At present, there is no consensus concerning the explanation of many experimental CISS results.[8]

Motivated by the CISS phenomena, we here address charge and spin currents in chiral molecular junctions within the framework of a minimal model. As a diagnostic tool of the junction's atomic structure, spin currents offer advantages as compared to charge currents: Spin polarized currents can, in principle, be detected in charge-transport measurements within an analyzer-polarizer setup employing, e.g., magnetized leads. However, they are expected to manifest themselves only in the non-linear regime and not in the linear charge conductance $G(\mathbf{M})$. This is a consequence of Onsager's reciprocity; its importance for the theory of the CISS effect was emphasized by Yang, van der Wal and van Wees.[9,10] [i] The spin-conductance, on the other hand, is less restricted by Onsager symmetries. It can be inferred, at least in principle, from measuring the pile-up of magnetization, e.g., in source or

---

[i]As is well known, due to the Onsager relations magnetotransport experiments based on the polarizer-analyzer setup will not detect spin-currents in the linear transport regime: even if a non-vanishing spin-current is flowing, the charge conductance is independent of the magnetization direction $G(\mathbf{M}) = G(-\mathbf{M})$ and therefore insensitive to the flow of spin.

drain. A brief review of the symmetry properties of transport coefficients is available in the Supporting Information, Sec. S1.

These considerations motivated us and other researchers[11] to investigate a minimal model for a chiral molecule in the presence of spin-orbit interactions. While Ref.[11] has focussed on the effect of contact-enhanced SOI, we adopt the model proposed by Michaeli and Naaman;[12] it exhibits SOI on the entire molecule and has the extra benefit of allowing for an analytical treatment. While Michaeli and Naaman have studied the transmission properties, our focus is on (spin) conductances. As one would have expected, the spin conductance turns out to be non-vanishing due to spin-orbit coupling. As a consequence, the transmitted and reflected currents tend to build up a non-vanishing spin-accumulation near both contacts, source and drain, already in the linear regime.[13] In stationary non-equilibrium the magnitude of induced magnetization is likely controlled by spin-relaxation processes. We predict the orientation of the magnetization in both contacts to be the same, in agreement with requirements of time-reversal invariance (TRI).[11]

Our work is of potential impact for constructing a molecular machine. Since total angular momentum is conserved by the LS-coupling, spin-flip processes exert a mechanical torque that can drive an engine. An analogue driving mechanism based on angular transfer has been investigated in Ref.[14]

Results

Minimal modeling of a helical molecule

Following Michaeli and Naaman[12] we consider electrons bound to a long tube. The left and right side of the tube are of cylindrical shape and represent (semi-infinite) reservoirs; the central region in between takes a helical shape to mimic a chiral molecule, see Fig. 1.

The Schrödinger equation that describes the free motion of a particle inside the helical

tube reads

$$\left[-\frac{\hbar^2 \boldsymbol{\nabla}^2}{2m_e} + V_{\mathrm{H}}(\mathbf{r}) + \frac{\mathrm{i}\hbar^2}{4m_e^2 c^2}\boldsymbol{\sigma} \cdot \boldsymbol{\nabla} V_{\mathrm{H}}(\mathbf{r}) \times \boldsymbol{\nabla}\right]\Psi(\mathbf{r}) = E\Psi(\mathbf{r}), \tag{1}$$

where $\mathbf{r}$ is the position vector in three dimensions; $V_{\mathrm{H}}(\mathbf{r})$ denotes an effective single-particle potential that confines the electron to the tube (see Fig. 1) with tube radius d, helical radius R and pitch b. The third term in the square brackets represents the spin-orbit interaction (SOI).

In the limit of small $d/\tilde{R}$ the electronic wavefunction is tightly bound to the helix and the quasi one-dimensional nature of the model becomes manifest; here, $\tilde{R} = \sqrt{(2\pi R)^2 + b^2} > 0$ denotes the distance covered when completing one helical turn. In this limit, the longitudinal and transverse motion approximately decouple and the problem simplifies. Following this idea, a systematic expansion of Eq. (1) in $d/\tilde{R}$ has been performed by Michaeli and Naaman [12] and keeping only leading order terms a minimal model has been derived.

Limit of a narrow tube

Wavefunction factorization

The wavefunction $\Psi(s, \varrho, \theta)$ can be conveniently expressed in a local cylindrical coordinate system: s denotes the longitudinal coordinate (distance along the helix); the motion in the plane normal to the tangential vector $\hat{\mathbf{s}}$ is described by the radial coordinate ϱ, which denotes normal distance from the center line of the tube (Fig. 1), and θ, which denotes the corresponding angular coordinate.

For simplicity, we will assume local rotational invariance in the sense $V_{\mathrm{H}}(\mathbf{r}) = V_{\mathrm{H}}(\varrho)$. In the small $d/\tilde{R}$ limit, the longitudinal and transverse motion nearly decouple, [12] and the wavefunction factorizes, [ii] $\Psi(s, \varrho, \theta) \approx \bar{\Psi}_m(s)\Phi_{N,m}(\varrho)\,e^{\mathrm{i}m\theta}$. The quantum number $N \in \mathbb{N}_0$ governs the nodal structure of the wavefunction in the radial direction. Due to the stipu-

---

[ii]The details of the confinement $V_{\mathrm{H}}(\varrho)$ are not relevant for the main conclusions of our work. Focusing on the lowest-energy eigenstates, we adopt a harmonic approximation $V_{\mathrm{H}}(\varrho) \approx \frac{1}{2}\frac{\hbar^2}{m_e d^4}\varrho^2$: the resulting wavefunctions $\Phi_{N,m}(\theta, \varrho)$ are eigenstates of a 2D harmonic oscillator with m-independent eigen-energies E_N and m restricted to $-N, -N+2, \ldots, N-2, N$.

lated rotational invariance, the $\hat{\mathbf{s}}$-component of the angular momentum, $-i\hbar\partial/\partial\theta$, is a good quantum number; we call it $\hbar m$ and $m \in \mathbb{Z}$. Finally, owing to the presence of SOI, $\bar{\Psi}_m(s)$ represents a two-spinor in spin-space.

In leading order, Eq. (1) turns to

$$\hat{H}_{N,m}(s)\bar{\Psi}_m(s) = E\bar{\Psi}_m(s),$$

where

$$\hat{H}_{N,m}(s) = E_N \; - \; \frac{\hbar^2}{2m_e}\left(\frac{\partial^2}{\partial s^2} \; + \; i\frac{2mb}{\tilde{R}^2}\frac{\partial}{\partial s}\right) \; + \; \hat{H}_{\mathrm{soi}}, \tag{2}$$

with E_N being the energy of the radial and angular motion. The second term on the right is the kinetic energy operator of the longitudinal motion. The third term couples momentum along s with the $\hat{\mathbf{s}}$-component of the orbital angular momentum, $\hbar m$. The origin of this term is geometric, it arises due to a non-zero pitch b of the helix. The last term, $\hat{H}_{\mathrm{soi}}$, is the SOI, which we simplify further in the following.

Spin-orbit coupling term

In the narrow-tube limit an expression for the spin-orbit term was given in the Ref.,[12]

$$\hat{H}_{\mathrm{soi}} = \kappa m\left[\hat{\sigma}_x \sin\left(\frac{2\pi\lambda s}{\tilde{R}}\right) - \hat{\sigma}_y \cos\left(\frac{2\pi\lambda s}{\tilde{R}}\right) - \hat{\sigma}_z\frac{b}{2\pi R}\right] \tag{3}$$

where $\kappa = \lambda(\hbar^4 R)/(4m_e^3 c^2 d^4 \tilde{R})$ and $\lambda = +1$ (-1) for a right (left) handed helix.

This expression adopts a transparent form on invoking a Cartesian representation

$$\hat{\mathbf{s}}(s) = -\frac{2\pi R}{\tilde{R}}\sin\left(\frac{\lambda 2\pi s}{\tilde{R}}\right)\hat{\mathbf{x}} + \frac{2\pi R}{\tilde{R}}\cos\left(\frac{\lambda 2\pi s}{\tilde{R}}\right)\hat{\mathbf{y}} + \frac{b}{\tilde{R}}\hat{\mathbf{z}}.$$

With $\mathbf{L} = m\hbar\hat{\mathbf{s}}$ it is easy to see that

$$\hat{H}_{\mathrm{soi}} = \beta\,\mathbf{L}\cdot\boldsymbol{\sigma}, \quad \beta = -\frac{\lambda\hbar^3}{8\pi m_e^3 c^2 d^4}. \tag{4}$$

As s increases along the helix, $\mathbf{L}(s)$ precesses around the z-direction. This spatial dependency of $\mathbf{L}(s)$ is the main entry point of helicity into the quasi-one-dimensional model. The precession of $\mathbf{L}$ invites an analogy with a magnetic moment $\boldsymbol{\mu}$ in a rotating magnetic field with "Zeeman energy" $|\boldsymbol{\mu} \cdot \mathbf{B}| = \hbar \beta m$ and $\mathbf{B} = B[\sin(\Omega s)\hat{\mathbf{x}} - \cos(\Omega s)\hat{\mathbf{y}} + B_z/B\,\hat{\mathbf{z}}]$; s being the effective "time" and oscillation frequency $\Omega = 2\pi/\lambda\tilde{R}$. Motivated by this observation, in the following paragraph we adopt a transformation to the rotating frame.[15]

Non-Abelian gauge transformation

To highlight the conservation of angular momentum in this model, we rewrite (4) introducing ladder operators

$$\hat{H}_{\text{soi}} = \beta \left[\hat{\sigma}_+ \hat{L}_-(s) + \hat{\sigma}_- \hat{L}_+(s) + \hat{\sigma}_z \hat{L}_z \right] \tag{5}$$

$$= \kappa m \left[\hat{\sigma}_+ \, \mathrm{i} e^{-\mathrm{i}\Omega s} - \hat{\sigma}_- \, \mathrm{i} e^{\mathrm{i}\Omega s} - \hat{\sigma}_z \frac{b}{2\pi R} \right] \tag{6}$$

where $\hat{\sigma}_\pm = (\hat{\sigma}_x \pm \mathrm{i}\hat{\sigma}_y)/2$ and $\hat{L}_\pm = \hat{L}_x \pm \mathrm{i}\hat{L}_y$.

In the representation (6), flipping the spin boosts the momentum along the tube axis by a reciprocal lattice vector $2\pi/\tilde{R}$. Alternatively to s, one can label the helical motion with an angle $\delta = \lambda 2\pi s/\tilde{R}$ that takes unique values on the entire real axis; moving up one pitch implies a change of $\delta \mapsto \delta \pm 2\pi$. From this perspective, the phase-factors in (6) boost the angular δ-dependency of the spinor $\Psi(\delta\frac{\lambda\tilde{R}}{2\pi}, \varrho, \theta)$ by an extra factor $e^{\mathrm{i}\delta}$, and in this sense angular momentum is conserved.

While the phase factor in (6) accounts for the conservation of the total angular momentum and therefore is crucial, it also obstructs an easy analytical solution of the model because it is not translationally invariant. The Hamiltonian considerably simplifies after a gauge transformation, $\bar{\Psi}_m(s) \mapsto e^{\mathrm{i}\lambda\hat{\sigma}_z \pi s/\tilde{R}}\bar{\Psi}_m(s)$, and accordingly for operators.[iii]

[iii] All operators transform as

$$\hat{A} \mapsto e^{\mathrm{i}\lambda\hat{\sigma}_z s\pi/\tilde{R}} \hat{A} e^{-\mathrm{i}\lambda\hat{\sigma}_z s\pi/\tilde{R}}.$$

The gauge-transformed Hamiltonian of the spin-orbit interaction follows from (6),

$$\hat{H}_{\text{soi}} \mapsto \hat{H}_{\text{soi}} = -\kappa m \left[\hat{\sigma}_y + \hat{\sigma}_z \frac{\lambda b}{2\pi R} \right]. \tag{7}$$

Whilst the term $\propto \hat{\sigma}_z$ in (6) remains invariant under the transformation, the rotating transverse components of the SOI in (6) collapse onto a single spatial direction, $\hat{\sigma}_y$. The latter direction does not follow from the geometry of the helix, but from our gauge-choice that associates the identity operator with the position $s = 0$.

Minimal model Hamiltonian

The effect of the gauge transformation on the longitudinal momentum operator is given by a spin-dependent "boost" $-\mathrm{i}\partial/\partial s \mapsto -\mathrm{i}\partial/\partial s - \frac{\lambda\pi}{\tilde{R}}\hat{\sigma}_z$. Along with (7) the application of the gauge transformation to the Eq. (2) leads to

$$\hat{H}_{N,m}(s) \mapsto \hat{H}_{N,m}(s) = \frac{\hbar^2}{2m_e} \left(-\mathrm{i}\frac{\partial}{\partial s} - \lambda\frac{\pi}{\tilde{R}}\hat{\sigma}_z + \frac{mb}{\tilde{R}^2} \right)^2 - \kappa m \left(\hat{\sigma}_y + \hat{\sigma}_z \frac{\lambda b}{2\pi R} \right) \tag{8}$$

where we discarded E_N and a constant $|m|$-dependent energy shift. The analysis simplifies upon introducing dimensionless variables $\hat{H}_{N,m} = \frac{\hbar^2\pi^2}{m_e\tilde{R}^2}\hat{H}'_{N,m}$ and $s = s'\frac{\tilde{R}}{\pi}$, leading to

$$\hat{H}'_{N,m}(s') = \frac{1}{2} \left(-\mathrm{i}\frac{\partial}{\partial s'} - \lambda\hat{\sigma}_z + \tilde{\gamma}m \right)^2 - \tilde{\kappa}m \left(\lambda\hat{\sigma}_y + \hat{\sigma}_z \frac{b}{2\pi R} \right). \tag{9}$$

In the above expression, $\tilde{\kappa} = \frac{\hbar^2 R\tilde{R}}{4\pi^2 m_e^2 d^4 c^2} > 0$ and $\tilde{\gamma} = \frac{b}{\pi\tilde{R}}$.

The $\tilde{\gamma}$-term corresponds to a momentum shift and thus represents a "synthetic" vector potential. It can formally be removed from $\hat{H}'_{N,m}$ by dressing the wavefunctions with a

---

To understand the action of the exponential operator on the spin raising and lowering operators in Eq. (6), one recalls that $\hat{\sigma}_+$ ($\hat{\sigma}_-$) annihilates spin up (spin down) states. Therefore the transformed operator

$$e^{\mathrm{i}\lambda\hat{\sigma}_z s\pi/\tilde{R}}\hat{\sigma}_+ e^{-\mathrm{i}\lambda\hat{\sigma}_z s\pi/\tilde{R}}$$

annihilates a spin-up state - as it would without being transformed - or equip a spin-down state with two times the same phase factor, i.e. $e^{2\mathrm{i}\lambda s\pi/\tilde{R}}$. As a consequence, the transformation indeed removes the phase factor of $\hat{\sigma}_+$ seen in Eq. (6).

gauge-factor $e^{i\tilde{\gamma}ms'}$,[16] and therefore leaves the spectrum invariant. If $\tilde{\gamma}m$ has a natural interpretation as a vector potential, the term proportional to b/R in the second line of (9) is the corresponding "synthetic Zeeman term". Notice that vector potential, $\tilde{\gamma}m$, and the Zeeman term change sign under $m \mapsto -m$; they do not break TRI because the full Hamiltonian sums over all m.

Dispersion relation

The model Hamiltonian (9) is straightforward to analyze. We focus on the effect of spin flips and therefore discard synthetic fields. Translational invariance of the Hamiltonian (9) suggests a representation in Fourier space

$$\hat{h}_m(k) = \frac{1}{2}\left(k - \lambda\hat{\sigma}_z\right)^2 - \lambda\tilde{\kappa}m\hat{\sigma}_y. \tag{10}$$

The model (10) exhibits a two-band dispersion $E_{m,\alpha}(k)$, where $\alpha = \pm 1$; see Supporting Information, Sec. S2, for explicit expressions.

Fig. 2 shows the dispersion law; the horizontal shift of the two parabolæ, red and blue, reflects the non-Abelian gauge transformation. The spin-orbit term is effective only at the crossing of parabolæ, where it opens a spin-orbit gap, $2|m|\tilde{\kappa}$, as is easily confirmed by degenerate perturbation theory at the crossing point $k = 0$. Chirality-induced spin-selective phenomena are expected to be strong in this region of energies.

In the gap region there remain four ungapped bands, - a factor of two for spin and angular momenta each, - where the spin projection and the sign of the velocity, $dE_{m,\alpha}(k)/dk$, are locked. In all four bands, the projection of spin onto the direction of velocity equals $-\lambda$ ("spin-momentum locking"). Such states are termed *helical*, in full analogy to the helicity concept for edge states in the quantum spin Hall effect.[17] The band-structure arising from (10) was also discussed in the context of Rashba quantum wires[18,19] and chiral carbon nanotubes,[20] although the physical origin of the terms of the Hamiltonain was different from our

situation. Specifically, the gap of the minmal model (7) opens due to the SOI term, $-\lambda\tilde{\kappa}m\hat{\sigma}_y$, while in Rashba wires and nanotubes such term originated from a transverse magnetic field.

Spin and charge transport

Molecule bound to straight tubes

To facilitate transport studies, we attach two straight tubes, Fig. 1, which serve as reservoirs. Formally, the reservoirs are included by extending the model (9), so that $\tilde{\gamma}, \tilde{\kappa} = 0$ if $s' < 0$ or $s' > L$. Importantly, the non-Abelian gauge transformation restores translational invariance also after attaching leads provided that it is performed in the reservoirs, too. Similarly, the synthetic vector potential, $\tilde{\gamma}(s')m$, can still be removed by applying a (non-local) gauge factor $e^{im\tilde{\Gamma}(s')}$, with $\tilde{\gamma}(s') = \partial_{s'}\tilde{\Gamma}(s')$.

Basic definitions

A finite bias drop $\mu_{\mathfrak{L}} - \mu_{\mathfrak{R}} = eV$ causes the flow of charge and spin, described by the charge current $I(V)$ and spin currents $I_i^{(\mathfrak{L})}(V)$, $I_i^{(\mathfrak{R})}(V)$ in each lead and each spatial direction $i = x, y, z$. Charge conductance G and spin conductances $G_i^{(\mathfrak{L})}, G_i^{(\mathfrak{R})}$ are defined by the linear response relations

$$I(V) = GV + \mathcal{O}(V^2) \tag{11a}$$

$$I_i^{(\mathfrak{L})}(V) = G_i^{(\mathfrak{L})}V + \mathcal{O}(V^2) \tag{11b}$$

$$I_i^{(\mathfrak{R})}(V) = G_i^{(\mathfrak{R})}V + \mathcal{O}(V^2) \tag{11c}$$

Due to local charge conservation, the charge current is well defined and, in particular, independent of where it is measured along the current flow. In contrast, spin is not locally conserved in the presence of spin-orbit coupling. It is only in the leads of the extended model where (longitudinal) spin-currents are well defined observables. Notice that due to the loss of spin-conservation in the central region, $0 < s < L$, spin-currents in left- and right-

reservoirs, $I_i^{(\mathfrak{L})}$ and $I_i^{(\mathfrak{R})}(V)$, may differ in a quasi-stationary non-equilibrium situation.

We adopt here the following sign convention for the spin currents: The $I_i^{(\mathfrak{L})}$ measures spin entering the junction from the left ($\mathfrak{L}$) contact and $I_i^{(\mathfrak{R})}(V)$ measures spin exiting the junction into the right ($\mathfrak{R}$) contact. This is fully analogous to the definition of the charge current.

Transmissions and Landauer Formulæ

The Landauer formalism relates conductances to the spectral transmission probabilities: for the transmission from $\mathfrak{R}$ to $\mathfrak{L}$, $T_{\sigma\sigma',m}^{(\mathfrak{L}\mathfrak{R})}(E)$, and vice versa, $T_{\sigma\sigma',m}^{(\mathfrak{R}\mathfrak{L})}(E)$, and to the corresponding reflection amplitudes, $R_{\sigma\sigma',m}^{(\mathfrak{L}\mathfrak{L})}(E)$ and $R_{\sigma\sigma',m}^{(\mathfrak{R}\mathfrak{R})}(E)$; see Ref. [21] for an overview. Here, the right (left) subscripts and superscripts of the transmission probability label the quantum numbers of an incoming (outgoing) wave, respectively. For example, $T_{\uparrow\downarrow,m}^{(\mathfrak{R}\mathfrak{L})}$ denotes the probability to transmit an electron with spin down from the left lead to the right one while flipping its spin in eigenchannel m. The charge conductances and the z-components of the spin conductances are given by

$$G = \frac{e^2}{h} \sum_m \sum_{\sigma\sigma'} T_{\sigma\sigma',m}^{(\mathfrak{R}\mathfrak{L})}(E_{\mathrm{F}}), \tag{12a}$$

$$G_z^{(\mathfrak{R})} = \frac{e}{4\pi} \sum_m \sum_{\sigma\sigma'} \sigma T_{\sigma\sigma',m}^{(\mathfrak{R}\mathfrak{L})}(E_{\mathrm{F}}), \tag{12b}$$

$$G_z^{(\mathfrak{L})} = \frac{e}{4\pi} \sum_m \sum_{\sigma\sigma'} (-\sigma) R_{\sigma\sigma',m}^{(\mathfrak{L}\mathfrak{L})}(E_{\mathrm{F}}) \tag{12c}$$

$$= \frac{e}{4\pi} \sum_m \sum_{\sigma\sigma'} \sigma T_{\sigma\sigma',m}^{(\mathfrak{L}\mathfrak{R})}(E_{\mathrm{F}}), \tag{12d}$$

where E_{F} indicates the Fermi energy (the Supporting Information, Sec. S5, offers a standard derivation within the scattering formalism). The expression for G chosen here emphasizes transmission of all spin species from left to right. From that expression the right spin conductance is obtained by multiplication by $\frac{1}{e}\frac{\hbar}{2}\sigma$ in the right lead. The left spin conductance expressed in the Eq. (12c) can then be understood as due to the reflected flux in the $\mathfrak{L}$-lead.

Particle conservation (unitarity, see Supporting Information, Sec. S4), leads to the equivalent form, Eq. (12d).

Transport Results

We address the transport problem by calculating the scattering matrix using conventional wavefunction matching. In this process, angular momentum m matches at the two interfaces: it is conserved in the scattering process; for further details see Supporting Information.

As example we focus on $N = 1$, so that $m = \pm 1$. We further continue to ignore the effect of the synthetic fields. In passing, we briefly mention that their effect is to assign a preferred spin direction, up or down, to a given angular momentum m. Hence, they will result in a circulating (transverse) spin current. In the following our focus is on the longitudinal currents.

The energy dependence of the resulting conductances for charge and spin in this model is displayed in Fig. 3. We offer a few comments:

- With E_{F} well outside the spin-orbit gap, the effect of spin-orbit coupling is small and translational invariance is hardly broken. In this case, back-scattering is weak and the (charge) conductance reaches a maximum of four conductance quanta reflecting two spin and two orbital ($m = \pm 1$) channels.

- In the off-gap regime mesoscopic oscillations are visible. The oscillation frequency (in E_{F}) is seen to decrease with the inverse length, L^{-1} and therefore we assign the oscillations to Fabry-Pérot interference.

- With E_{F} inside the spin-orbit gap, backscattering inside the the wire is suppressed and the Fabry-Pérot oscillations quickly die out.

- In the in-gap regime, electrons can tunnel via two evanescent modes that result from the two 'gapped' bands. Accordingly, the charge conductance in the middle of the gap approaches 2 conductance quanta from above.

- The absolute value of the spin conductances in either one of the leads approaches $2\frac{e}{4\pi}$. This can be understood from Fig. 2: in the spin-orbit gap the right (or left) moving modes have identical spin regardless of m, *i.e.* there are two channels distinguished only by the orbital angular momentum.

- Importantly, the spin conductances are non-zero for energies even far from the spin-orbit gap, where the oscillations peak at $\approx 0.2\frac{e}{4\pi}$. It can be shown that that $G_x^{(\mathfrak{L},\mathfrak{R})}(E_F) = 0$ for any E_F since the Bloch functions have zero average $\hat{\sigma}_x$. Moreover, $G_y^{(\mathfrak{L},\mathfrak{R})} = 0$ because the expectation values of $\hat{\sigma}_y$ change sign along with the sign change of m (see Fig. 2), while the lead Hamiltonian is m-independent. In other words, the y components of outgoing waves exactly cancel upon the summation over m.

- Remarkably, the $\mathfrak{L}$ and $\mathfrak{R}$ spin conductances differ only up to a sign. By combining TRI and left-right reflection it is possible to derive relations between scattering matrix elements that lead to the exact identity $G_z^{(\mathfrak{R})} = -G_z^{(\mathfrak{L})}$ at any energy. (See Supporting Information, Sec. S4,S5 for the details of this symmetry analysis.) In realistic molecular junctions a symmetry of couplings to the left and right leads can not be expected. We show in the next section that in this more general situation, the magnitude of $G_z^{(\mathfrak{R})}$ and $G_z^{(\mathfrak{L})}$ no longer is the same, while the sign is still opposite due to TRI.

Qualitative understanding of spin transport

A frequent misconception

We begin the discussion by addressing a common misconception of the minimal model: Fig. 2 is frequently interpreted as predicting a nonzero spin current even in equilibrium. Indeed, Fig. 2 seems to suggest that for a Fermi level situated in the spin-orbit gap there is an excess of spin-up right movers (velocity $dE_{m,\alpha}(k)/dk > 0$) over spin-down right movers. Taken at face value this observation would imply that due to the wire connecting $\mathfrak{L}$ and $\mathfrak{R}$ reservoirs, both reservoirs would become magnetized at equilibrium. Clearly, such a

transport of magnetization is violating the second law of thermodynamics. The vanishing of equilibrium spin currents is a rigorous consequence of unitarity, see Supporting Information, Sec. S5. The fact that spin transport can not be derived from the band-structure alone is known in the field of two-dimensional materials, see Sec. 4.1 of Ref.[23] for a review and a discussion in the context of CISS in Ref.[9] The paradox will be resolved on a more intuitive level in the subsequent discussion.

Long helix limit

We consider $\lambda = -1$ and the limit $L \gg d, R$ and Fermi energy, E_{F}, inside the spin-orbit gap. In this limit, at observation points deep inside the one-dimensional wire all up-spin fermions flow one direction, while all down-spin fermions flow into the other direction, see Fig. 2. We infer that $T_{\downarrow\downarrow,m}^{(\mathfrak{L}\mathfrak{R})}, T_{\uparrow\uparrow,m}^{(\mathfrak{R}\mathfrak{L})} \simeq 1$; there is no spin-flip inside the wire. On the other hand, deep inside either reservoir the spin-orbit gap vanishes. Therefore, spin-up and spin-down currents flow alike in either direction. It is easy to see that both limits match if $R_{\uparrow\downarrow,m}^{(\mathfrak{L}\mathfrak{L})}, R_{\downarrow\uparrow,m}^{(\mathfrak{R}\mathfrak{R})} \simeq 1$.

The situation is illustrated in Fig. 4(a). The central region of the junction shows counter-propagating electrons with opposite spin, as suggested by Fig. 2. These modes are properly interpreted as carrying a conductance quantum for charge, because charge is conserved inside the wire; hence, in Fig. 3 the conductance is seen to be $G \approx e^2/h$ per angular-momentum channel inside the gap. These same modes are not properly interpreted in terms of spin-conductances, however, because spin is not conserved inside the wire.

The propagation pattern of current channels in the leads is also displayed in Fig. 4(a); the matching condition at the interface shown there follows from bulk limits. Since spin is conserved inside the reservoirs, the channel pattern may be interpreted in terms of spin currents. As one would expect, there are no net spin currents inside the reservoirs in equilibrium, because the propagating spin-current is exactly compensated by the (reflected) counter-propagating current.

Upon applying a finite bias, states with energy inside the bias window are incoming only

from one reservoir. In this case a spin current of one spin-conductance quantum (per angular momentum channel) survives inside the reservoirs. Also with respect to spin-conductances the Fig. 4(a) and Fig. 3 provide a consistent picture.

The qualitative discussion given here is fully backed up by an explicit calculation of all scattering probabilities; for explicit results, we refer the reader to the Supporting Information, Figure S2.

Reservoirs accumulating spin

An implication of spin-flip scattering is that both reservoirs accumulate spin in the presence of a current flow. To see how this happens we once again consult Fig. 4(a). For a charge current flowing from $\mathfrak{L}$ to $\mathfrak{R}$, the drain acquires a spin up magnetization (red). Simultaneously, the incoming flow of spin down particles (blue) is reflected and spin flipped, so that the $\mathfrak{L}$-lead acquires a spin up magnetization (red), too. The observation represents a one-dimensional analogue of the Rashba-Edelstein effect.[24]

The parallel magnetizing of both leads is formally expressed by the anti-symmetry of spin conductances

$$G_z^{(\mathfrak{R})} = -G_z^{(\mathfrak{L})}. \tag{13}$$

The identity can be proven to hold under general conditions (*e.g.* at arbitrary energy) provided the coupling to both leads is symmetric. We present a formal proof in the Supporting Information, Sec. S5. Importantly, if mirror symmetry is broken, the sign of conductances remains opposite, as we demonstrate in the next section below.

Comparison to a spin filter

For further illustration, we confront the spin-flip scattering in the helical junction with the more familiar case of a magnetized junction that operates as a spin-filter, Fig. Fig. 4(b). Also in this archetypal situation the reservoirs accumulate spin, however they do so in opposite directions (see the schematics of scattering in Fig. 4). The key difference to the previous case

is that spin is conserved everywhere, so that the (minority) spins removed from the source accumulate in the drain.

Magnetizing reservoirs with imperfect contacts

Realistic molecular junctions exhibit contact resistances that are not included in the minimal model. To investigate the effect of contact imperfections we add a potential term to the $\mathfrak{L}$ contact,

$$v(s') = c\,\delta(s')\cdot\hat{\sigma}_0. \tag{14}$$

This potential barrier is readily built into the scattering formalism as a modification of the matching conditions between the wire and the leads (Supporting Information, Sec. S3).

Fig. 5 displays the conductances for increasing barrier strength. The charge conductance exhibits a gradual cross-over from the transparent, weak-barrier limit, $c \ll 1$, to the strong-barrier limit, $c \gg 1$, in which the transmission grows linearly with E_F. Concomitantly, the spin-conductances evolve in a strikingly asymmetric fashion. For qualitative insight to the strong barrier limit we consult again Fig. 4(a). For a current flowing from $\mathfrak{L}$ to $\mathfrak{R}$ and E_F inside the spin-orbit gap, the barrier suppresses the transmitted current and spin-flip processes alike; hence, $G_z^{(\mathfrak{L})}$ is strongly suppressed inside the source. Conversely, the spin-current flowing in the drain equals the transmitted current (in units of the conductance quanta). Our argument implies that the spin conductances continue to exhibit opposite signs in the presence of asymmetries. Therefore, we propose that the property of source and drain to magnetize into the same direction upon a current flowing is a general result robust with respect to generic deformations of the minimal model (14).

Beyond the minimal model: Spin-flip reflection processes

The qualitative analysis of scattering from the Fig. 4 indicates that spin-flipping reflections play a crucial role in the spin transport within the minimal model. Indeed, within our phase coherent approach we can cast the spin conductances into the form

$$G_z^{(\mathfrak{R})} = \frac{e}{4\pi} \sum_m \left(R_{\downarrow\uparrow,m}^{(\mathfrak{R}\mathfrak{R})} - R_{\uparrow\downarrow,m}^{(\mathfrak{R}\mathfrak{R})} \right) \tag{15}$$

$$G_z^{(\mathfrak{L})} = \frac{e}{4\pi} \sum_m \left(R_{\downarrow\uparrow,m}^{(\mathfrak{L}\mathfrak{L})} - R_{\uparrow\downarrow,m}^{(\mathfrak{L}\mathfrak{L})} \right) \tag{16}$$

(see Supporting Information, Sec.S5.3). This expression demonstrates that spin conductances and reflections are closely related to each other; one cannot exist without the other.

Note that these formulæ are independent on the details of the junction's Hamiltonian and only assume the presence of two orbital channels, labelled by m, related by TRI. Therefore it is not surprising that the close connection between spin-currents and reflectivities also holds in other models. For instance, Yang, van der Wal and van Wees have demonstrated within an incoherent single channel model that spin-flip reflections must be non-zero for spin-currents to exist in a chiral TRI conductor.[9]

Induced spin and charge densities in the contact

We supplement the transport results with expressions for the charge and spin density in the $\mathfrak{L}$-lead ($s < 0$) in linear response. The latter quantities will be given in units of e and $\hbar/2$, respectively. Our formulæ follow from scattering theory and are thus independent on the microscopic details of the Hamiltonian. The details of the derivation are moved to Supporting Information, Sec. S6, for the sake of brevity.

The charge density evaluates to the expression

$$n(s) = n(s)\Big|_{V=0} + V \varrho_L(E_F) \left[\left(4 - \frac{h}{e^2}G \right) + 2\sum_m \mathrm{Re}\left\{ e^{-\mathrm{i}2qs} r_{\uparrow\uparrow,m}^{(\mathfrak{L}\mathfrak{L})} \right\} \right]_{E=E_F} + \mathcal{O}(V^2). \tag{17}$$

where $r_{\uparrow\uparrow,m}^{(\mathfrak{L}\mathfrak{L})} = r_{\downarrow\downarrow,-m}^{(\mathfrak{L}\mathfrak{L})}$ has been used reflecing TRI (see also Supporting Information, Sec. S6). The first term is the equilibrium charge density; as shown in Supporting Information, Sec. S6.2, it reveals a familiar contact Friedel oscillation caused by quantum interference with reflected waves in a Fermi ground-state.

In the linear response term in (17) we factored out the expression

$$\varrho_{\mathrm{L}}(E_{\mathrm{F}}) = \frac{1}{2\pi} \sum_{q>0} \delta\left(E_{\mathrm{F}} - \frac{q^2}{2}\right) = \frac{1}{4\pi^2 q_{\mathrm{F}}}, \tag{18}$$

being a (homogeneous) local density of states of right movers (per spin) in a single channel homogeneous wire. The square brackets in Eq. (17) contain two terms: a homogeneous (s-independent) term, $\left(4 - \frac{h}{e^2}G\right)$, represents the enhancement of the charge-density that is associated with the reflected particles. The reflection-induced enhancement of the charge density also leaves a trace in the Friedel-oscillations, which is expressed by the second term.

Notice that unlike spin-conserving processes, spin-flip processeses, such as incorporated by $r_{\downarrow\uparrow,m}^{(\mathfrak{L}\mathfrak{L})}$, do not contribute to the oscillating term in (17) because the superposition of two probability currents with opposite spins has no cross (interference) term. Spin-flip terms do enter the conductance, G, of course.

The induced spin density in the left lead reads

$$n_z(s) = -V \, \varrho_{\mathrm{L}}(E_{\mathrm{F}}) \frac{4\pi}{e} G_z^{(\mathfrak{L})} + \mathcal{O}(V^2); \tag{19}$$

there is no spin density in equilibrium because of TRI. The (linear) spin imbalance represents the the loss of spin-density associated with the transmitted spin-current. For this reason, Eq. (19) implies that a measurement of the linear response of the local spin-density yields (up to trivial factors) the transport coefficient $G_z^{(\mathfrak{L})}$. Notice that in striking contrast to the charge density, the spin density does not display Friedel oscillations even in linear response; ultimately, as we show in the Supplementary Information, the reason is TRI.

We further note that the current-induced spin-accumulation, (19), goes hand in hand

with a spin-split chemical potential if a self-consistent description of the quasi-static non-equilibrium situation is employed:[25]

$$\mu_\uparrow^{(\mathfrak{L})}(V) - \mu_\downarrow^{(\mathfrak{L})}(V) = -V\frac{\pi}{2e}G_z^{(\mathfrak{L})} + \mathcal{O}(V^2); \qquad (20)$$

the formula follows from (19) and is also derived in the Supplementary Information, Supporting Information, Sec. S6. We offer two comments on this expression: First, the coefficient multiplying V can reach $\frac{1}{4}$ if E_F lies in the SOI gap, *i.e.* the spin accumulation is non-perturbative in the SOI strength. Second, assuming that the reservoirs ultimately relax spin (and charge), but do not introduce backscattering, the spin accumulations can be measured in the vicinity of the contact by a four-terminal setup, or by Hanle spin precession, as suggested by Yang, van der Wal and van Wees.[10,26]

Further remarks

- The (experimental) measurement of spin currents and spin accumulation is a central topic in the field of *Spintronics*.[27,28] In particular, the possibility of spin accumulation near interfaces between materials with and without spin-orbit interaction is well understood;[29] the results we here report on the minimal level confirm the validity of the general picture down to the molecular scale.

  In Sec. 2 we have mentioned that the bands for energies in the spin-orbit gap are analogous to edge states associated with a quantum spin Hall device. As a consequence, the minimal model exhibits spin-momentum locking with the consequence that backscattering off defects is suppressed. In other words, we expect that our transport results are robust against weak (non-magnetic) disorder.

- Recently, a related work on parallel spin-accumulation and spin transport has been published.[11] The tight-binding chain investigated by these authors is essentially equivalent to

our toy model with a distinctive difference: in Ref.[11] the SOI is confined to the contact bond, only, while in our toy model the SOI is a property of the molecule and non-vanishing along the entire helical structure.

The spin conductances reported in Ref.[11] show the same symmetry, $G_z^{(\mathfrak{L})} = -G_z^{\mathfrak{R}}$, as in our work. However, the energy dependences of the spin conductances exhibit pronounced differences: $G_z^{(\mathfrak{L}/\mathfrak{R})}(E)$ in Ref.[11] does not exhibit a fixed sign; in our case it does, so that the sign of the spin accumulation is independent of the Fermi energy. This difference can be traced back to the different ways how SOI is implemented; it may, at least in principle, be used to discriminate one situation from the other, experimentaly.

- It is well-known in Spintronics that spin conductances are non-zero in junctions with multiple conduction channels only (see Supporting Information, Sec. S1, Principle 1). In our model, the absence of spin polarization for a single channel is immediately obvious by setting $m = 0$ in Eq. (9). Molecular junctions generically exhibit multiple channels and are thus prepared for hosting spin currents (*e.g.* see Ref.[30] for a channel analysis of helical peptides). Frequently employed molecular linker units (*e.g.* thiol groups linked to Au) effectively suppress all conduction channels but one. Moreover, the generation of significant spin currents benefits from two conduction channels of similar transmission probabilities, which in turn requires quasi-degenerate molecular orbitals. To favor such conditions, linker-free benzene-type structures are natural candidates. They can be functionalized with heavier elements (see *e.g.* Ref.[31]) to boost the spin-orbit coupling and promote chirality.

Summary and conclusions

We have investigated charge and spin transport in a minimal model of a helical molecule with spin-orbit coupling attached to two spin-conserving leads. The minimal model was first devised by Michaeli and Naaman and allows for a full analytic treatment of transport

properties. While the earlier authors have focussed on spin polarizations, we calculated the full conductance matrix, including charge and spin conductances.

The band-structure of the minimal model hosts four helical bands that exhibit spin-momentum locking. We first clarify the connection between transport properties and band-structure. In particular, first glances could suggest the existence of an equilibrium spin current, which sometimes is used as an argument against the validity of the model. We explain the origin of the misunderstanding, which results from neglecting the contact scattering that always exists in a transport geometry. In actuality, there is no equilibrium spin transport in this model.

Our explicit calculation of charge and spin conductances in the Landauer formalism show that the spin conductance reaches a maximum $(e/2\pi)$ for energies inside the gap, corresponding to 2 fully polarized conduction channels. Outside the gap region the spin conductances remain sizable, too. Further, we find that at small biases and for incoming currents being unpolarized, there are spin currents with opposite signs in each lead.

Upon a current flowing, spin accumulates in the vicinity of each contact as a consequence of the spin currents; the magnetizations at left and right contacts are the same and reverse with voltage and helicity. The magnitude of the accumulated spin polarization is directly proportional to the spin conductance of the respective lead; therefore, we reveal a new route towards the measurement of $G_z^{(\mathfrak{L}/\mathfrak{R})}$, as has also been proposed for specific device geometries by Yang et $al.$[26]

We add a remark on spin-accumulation in mesoscopic systems: accumulated spins have a feedback on the transport currents in first order in the applied biases. In particular, spin accumulations can drive charge currents as well as charge currents can drive spin currents, reflecting an Onsager reciprocity. Seemingly, this reciprocity has not been widely appreciated in previous theories of the CISS effect.

The minimal model therefore directly reveals important features of analytic structure of spin transport in helical molecules. It can serve as a guidance for the interpretation of

ab-initio calculations of transport coefficients in chiral molecular systems, *e.g.*, based on nonequilibrium Green's functions. Further, it lends itself to straightforward generalizations, e.g., the analytic calculation of current-induced mechanical torques in a quantum model.

Methods

The band-structure of an infinite helical wire was obtained by diagonalizing the Eq. (10). Explicit analytic expressions are given in the Supporting Information, Sec. S2. The junction was modelled with a central helical element of length L attached to a pair of semi-infinite straight tubes (Fig. 1). Hamiltonian eigenstates were obtained by wavefunction matching, see Sec. S3. Spin conductances (12) were obtained from the scattering matrix in Landauer approach; the respective formulæ were re-derived in Sec. S5 for reference purposes. The local magnetization density was calculated from explicit wave-functions in presence of two chemical potentials, Sec. S6.

Acknowledgement

Supporting Information Available: The accompanying file contains supporting sections S1-S6 with methodological details.

References

1. Evers, F.; Korytár, R.; Tewari, S.; van Ruitenbeek, J. M. Advances and Challenges in Single-Molecule Electron Transport. Rev. Mod. Phys. **2020**, _92_, 035001.

2. Göhler, B.; Hamelbeck, V.; Markus, T. Z.; Kettner, M.; Hanne, G. F.; Vager, Z.; Naaman, R.; Zacharias, H. Spin Selectivity in Electron Transmission Through Self-Assembled Monolayers of Double-Stranded DNA. Science **2011**, _331_, 894.

3. Naaman, R.; Paltiel, Y.; Waldeck, D. Chiral Molecules and the Electron Spin. Nature Reviews Chem. **2019**, _3_, 250–260.

4. Liu, T.; Wang, X.; Wang, H.; Shi, G.; Gao, F.; Feng, H.; Deng, H.; Hu, L.; Lochner, E.; Schlottmann, P., et al. Linear and Nonlinear Two-Terminal Spin-Valve Effect from Chirality-Induced Spin Selectivity. ACS Nano **2020**, _14_, 15983–15991.

5. Safari, M. R.; Matthes, F.; Caciuc, V.; Atodiresei, N.; Schneider, C. M.; Ernst, K.-H.; Bürgler, D. E. Enantioselective Adsorption on Magnetic Surfaces. Advanced Materials **2023**, 2308666.

6. Safari, M. R.; Matthes, F.; Schneider, C. M.; Ernst, K.-H.; Bürgler, D. E. Spin-Selective Electron Transport Through Single Chiral Molecules. Small **2023**, 2308233.

7. Theiler, P. M.; Ritz, C.; Hofmann, R.; Stemmer, A. Detection of a Chirality-Induced Spin Selective Quantum Capacitance in α-Helical Peptides. Nano Lett. **2023**, _23_, 8280–8287.

8. Evers, F.; Aharony, A.; Bar-Gill, N.; Entin-Wohlman, O.; Hedegård, P.; Hod, O.; Jelinek, P.; Kamieniarz, G.; Lemeshko, M.; Michaeli, K., et al. Theory of Chirality Induced Spin Selectivity: Progress and Challenges. Adv. Mat. **2022**, _34_, 2106629.

9. Yang, X.; van der Wal, C. H.; van Wees, B. J. Spin-Dependent Electron Transmission Model for Chiral Molecules in Mesoscopic Devices. Phys. Rev. B **2019**, _99_, 024418.

10. Yang, X.; van der Wal, C. H.; van Wees, B. J. Detecting Chirality in Two-Terminal Electronic Nanodevices. Nano Lett. **2020**, 20, 6148–6154.

11. Wolf, Y.; Liu, Y.; Xiao, J.; Park, N.; Yan, B. Unusual Spin Polarization in the Chirality-Induced Spin Selectivity. ACS Nano **2022**, 16, 18601–18607.

12. Michaeli, K.; Naaman, R. Origin of Spin-Dependent Tunneling Through Chiral Molecules. J. Phys. Chem. C **2019**, 123, 17043–17048.

13. García-Blázquez, M.; Dednam, W.; Palacios, J. Nonequilibrium Magneto-Conductance as a Manifestation of Spin Filtering in Chiral Nanojunctions. J. Phys. Chem. Lett. **2023**, 14, 7931–7939.

14. Korytár, R.; Evers, F. Current-Induced Mechanical Torque in Chiral Molecular Rotors. Beilstein Journal of Nanotechnology **2023**, 14, 711–721.

15. Abragam, A. The Principles of Nuclear Magnetism; Oxford university press, 1961; Chapter II.B.

16. Geyer, M.; Gutierrez, R.; Cuniberti, G. Effective Hamiltonian Model for Helically Constrained Quantum Systems within Adiabatic Perturbation Theory: Application to the Chirality-Induced Spin Selectivity (CISS) Effect. J. Chem. Phys. **2020**, 152, 214105.

17. König, M.; Buhmann, H.; W. Molenkamp, L.; Hughes, T.; Liu, C.-X.; Qi, X.-L.; Zhang, S.-C. The Quantum Spin Hall Effect: Theory and Experiment. J. Phys. Soc. Japan **2008**, 77, 031007.

18. Sánchez, D.; Serra, L. m. c.; Choi, M.-S. Strongly Modulated Transmission of a Spin-Split Quantum Wire with Local Rashba Interaction. Phys. Rev. B **2008**, 77, 035315.

19. Středa, P.; Šeba, P. Antisymmetric Spin Filtering in One-Dimensional Electron Systems with Uniform Spin-Orbit Coupling. Phys. Rev. Lett. **2003**, 90, 256601.

20. Marganska, M.; Milz, L.; Izumida, W.; Strunk, C.; Grifoni, M. Majorana Quasiparticles in Semiconducting Carbon Nanotubes. Phys. Rev. B **2018**, _97_, 075141.

21. Jacquod, P.; Whitney, R. S.; Meair, J.; Büttiker, M. Onsager Relations in Coupled Electric, Thermoelectric, and Spin Transport: The Tenfold Way. Phys. Rev. B **2012**, _86_, 155118.

22. Bercioux, D.; Lucignano, P. Quantum Transport in Rashba Spin-Orbit Materials: A Review. Rep. Progr. Phys. **2015**, _78_, 106001.

23. Ref. 22, Sec. 4.1.

24. Edelstein, V. Spin Polarization of Conduction Electrons Induced by Electric Current in Two-Dimensional Asymmetric Electron Systems. Solid State Communications **1990**, _73_, 233–235.

25. Nazarov, Y. V.; Blanter, Y. M. Quantum Transport: Introduction to Nanoscience; Cambridge University Press, 2009.

26. Yang, X.; van Wees, B. J. Linear-response magnetoresistance effects in chiral systems. Phys. Rev. B **2021**, _104_, 155420.

27. Bardarson, J. H.; Adagideli, i. d. I.; Jacquod, P. Mesoscopic Spin Hall Effect. Phys. Rev. Lett. **2007**, _98_, 196601.

28. Adagideli, i. d. I.; Bardarson, J. H.; Jacquod, P. Electrical Probing of the Spin Conductance of Mesoscopic Cavities. Journal of Physics: Condensed Matter **2009**, _21_, 155503.

29. Adagideli, i. d. I.; Scheid, M.; Wimmer, M.; Bauer, G. E. W.; Richter, K. Extracting Current-Induced Spins: Spin Boundary Conditions at Narrow Hall Contacts. New Journal of Physics **2007**, _9_, 382.

30. Liu, Y.; Xiao, J.; Koo, J.; Yan, B. Chirality-Driven Topological Electronic Structure of DNA-Like Materials. Nature Mater. **2021**, _20_, 638–644.

31. Adachi, Y.; Ohshita, J. Germanium and Tin in Conjugated Organic Materials. <u>Main Group Strategies towards Functional Hybrid Materials</u> **2017**, 237–264.
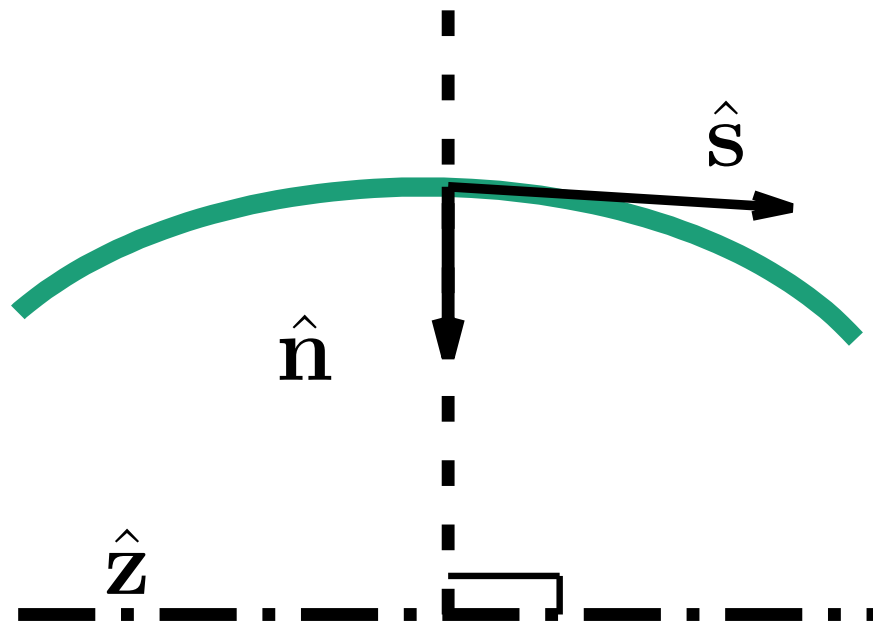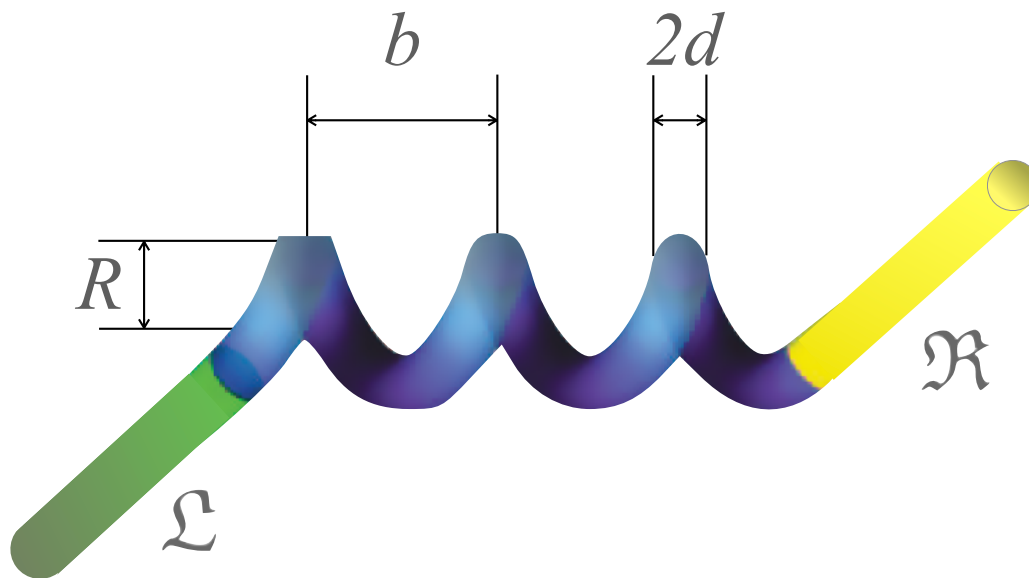
TOC Graphic
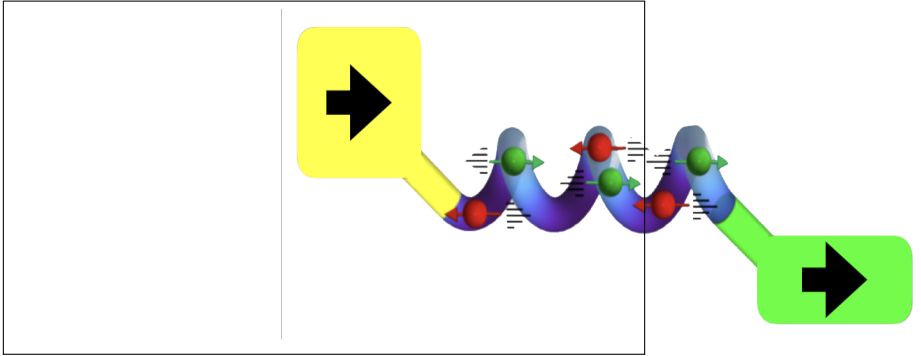
Figure 1: Top: Scheme of the molecular junction consisting of a helical tube (center) and a pair of semi-infinite straight tubes, left and right. The radius R, pitch b, thickness $2d$ are indicated. Bottom: Illustration of helical coordinates s, ϱ, θ: Green line shows part of a helix that evolves along the z axis (dash-dotted line) with unit vector $\hat{\mathbf{z}}$. At any given point on the helix, the unit vector $\hat{\mathbf{n}}$ is perpendicular to $\hat{\mathbf{z}}$ and the unit tangent vector $\hat{\mathbf{s}}$. In helical coordinates, s is the distance along the helix; θ and ϱ are polar coordinates in a plane normal to $\hat{\mathbf{s}}$; θ measures from $\hat{\mathbf{n}}$.
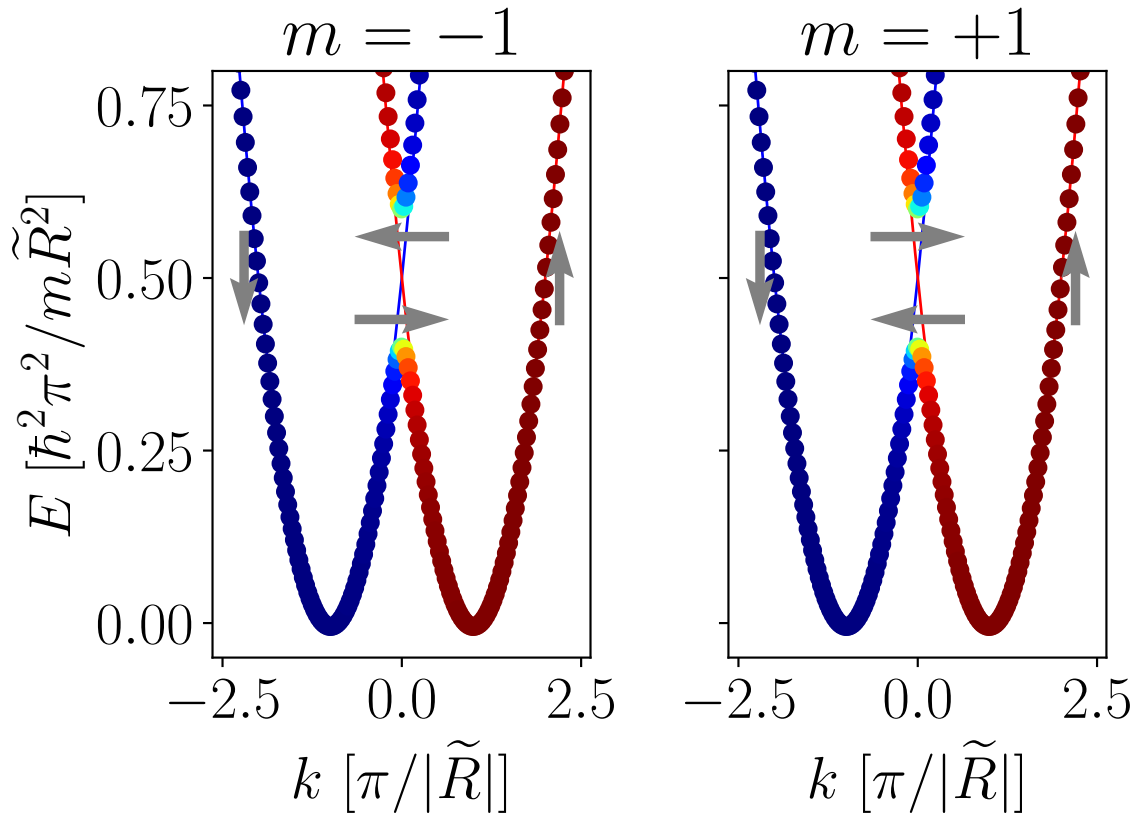
Figure 2: Dispersion relation of the helical tube for $m = +1$ and -1 is shown with dots. Color indicates the expectation value of $\hat{\sigma}_z$ (red=+1, blue=-1, green=0). Grey arrows represent the expectation value of spin in the yz-plane [$\hat{\sigma}_y$ ($\hat{\sigma}_z$) is the horizontal (vertical) component, respectively]. For comparison, the thin solid lines depict the dispersion of a straight tube. The horizontal spin-dependent shift of the parabolæ reflects the non-Abelian gauge transformation. Parameters: $\tilde{\kappa} = 0.1, \lambda = -1$. The eigen-energies are m-independent.
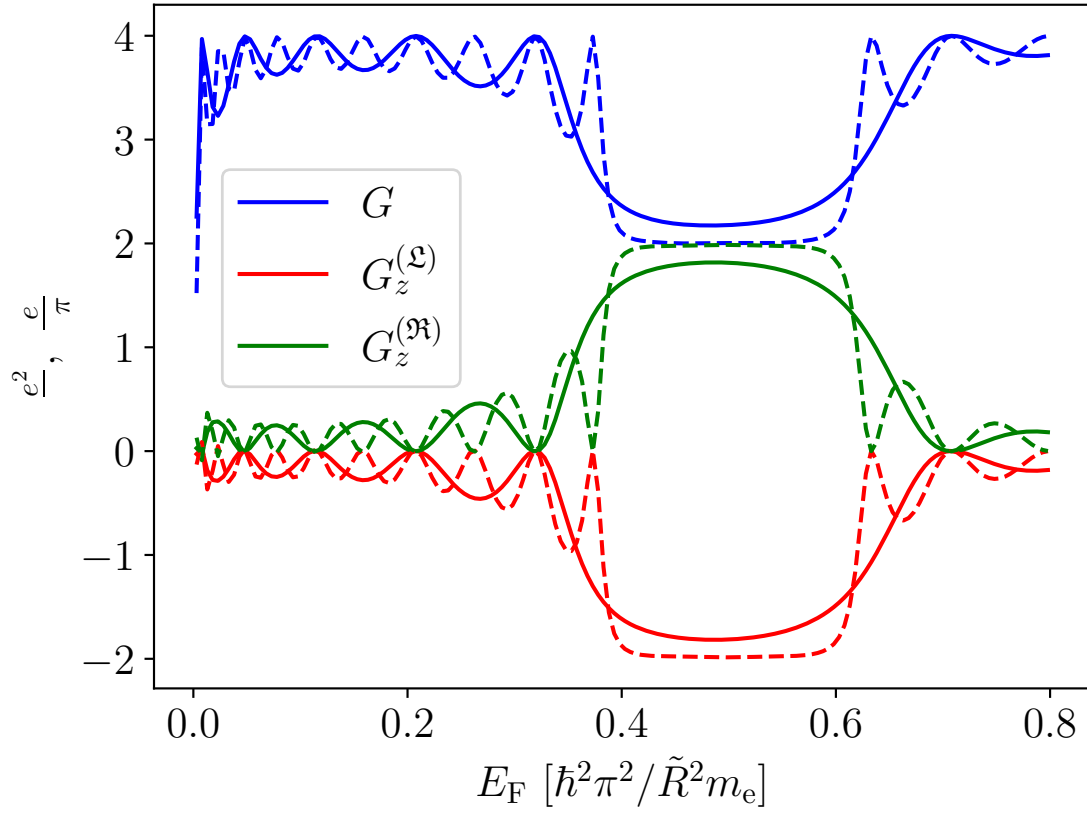
Figure 3: Charge conductance and the z-components of the spin conductances in the Michaeli model as a function of the Fermi energy E_{F}. Solid (dashed) lines are for a helix with 3 (dashed) and 6 (solid) turns. Parameters are the same as in Fig. 2, with a spin-orbit gap between 0.4 and 0.6.
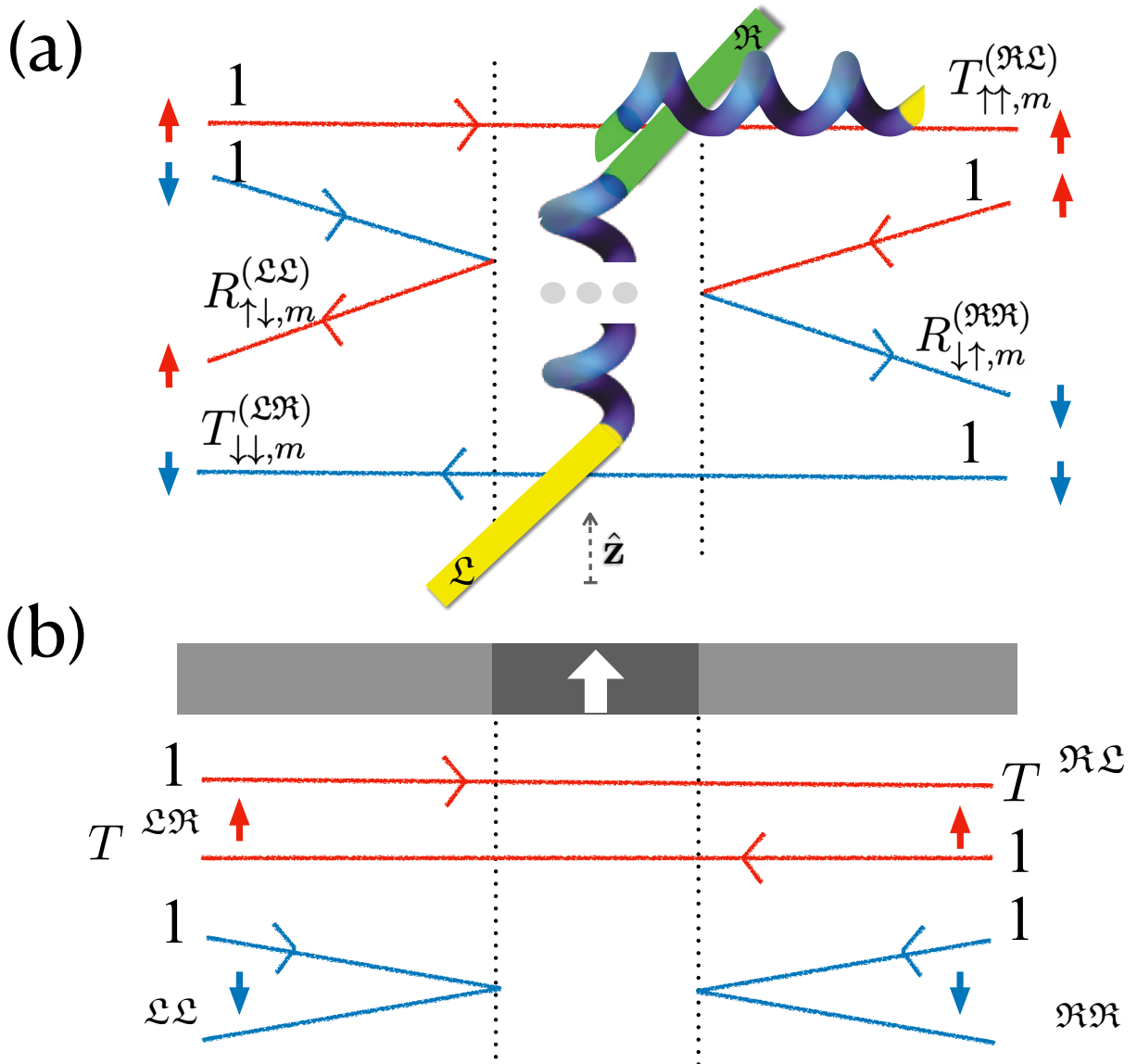
Figure 4: Schematic representation of scattering processes in the helical junction (a) and a ferromagnetic polarizer (b). Panel (a) applies in the limit of a long helix (helicity $\lambda = -1$) for energies in the spin-orbit gap. Red (blue) color indicates spin up (down) in the sense of the helical axis. The red line on the top indicates that the electron with spin $\uparrow$ coming from the left ($\mathfrak{L}$) lead (normalized to probability 1) is transmitted and its spin is conserved. If the incoming electron has spin $\downarrow$, it is reflected with a spin-flip due to TRI. Panel (b) illustrates scattering off an ideal ferromagnetic polarizer that only transmits spin up electrons.
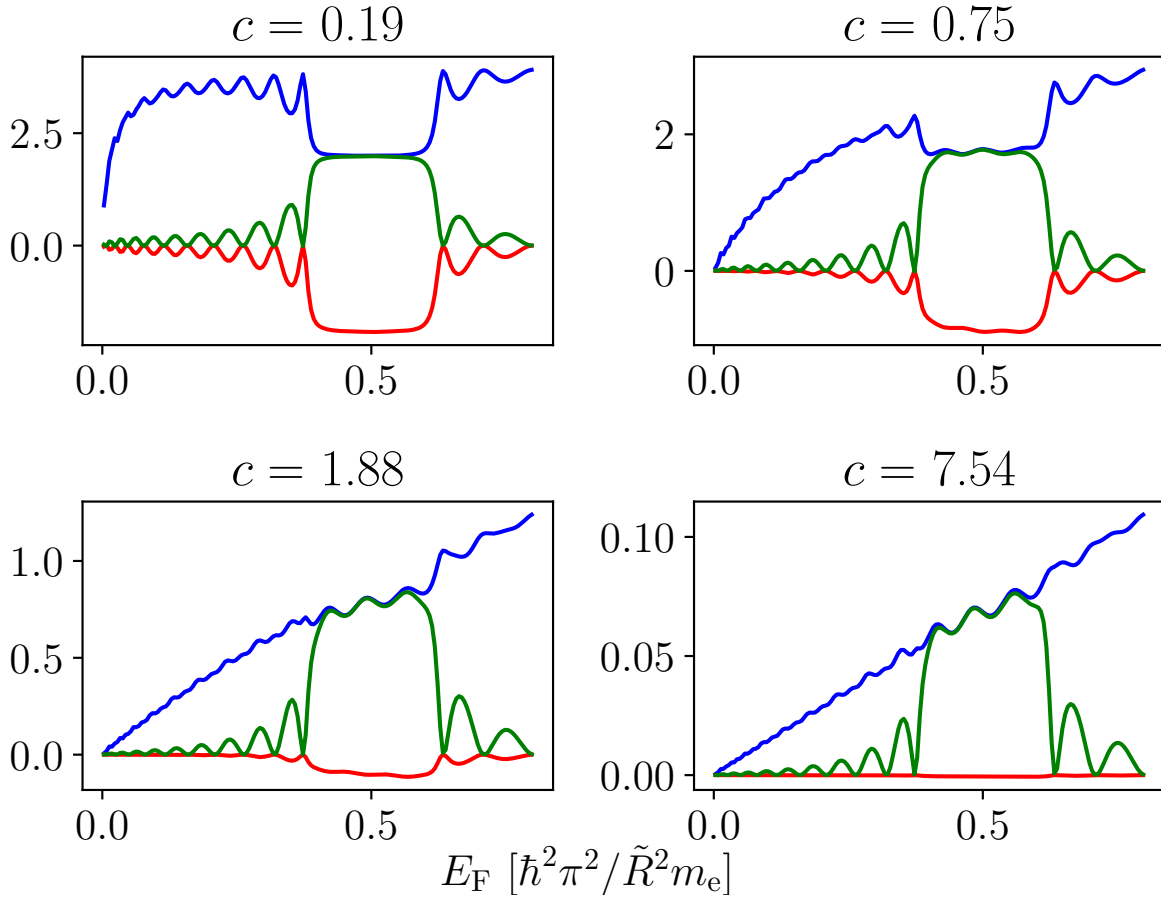
Figure 5: Plot similar to Fig. 3 illustrating the sensitivity of charge and spin conductances, $G/\frac{e^2}{h}$ (blue), $G_z^{(\mathfrak{R}/\mathfrak{L})}/\frac{e}{4\pi}$ (green/red) to the contact imperfection (14) for a helical wire with 6 turns. The panels differ by increasing strength of the potential barrier c at the left contact.

Spin conductances and magnetization production in chiral molecular junctions: Supplementary Information

Richard Korytár,[*],[†] Jan M. van Ruitenbeek,[‡] and Ferdinand Evers[¶]

†*Department of Condensed Matter Physics, Faculty of Mathematics and Physics, Charles University, Ke Karlovu 5, 121 16, Praha 2, Czech Republic*

‡*Huygens-Kamerlingh Onnes Laboratory, Leiden University, NL-2333CA Leiden, Netherlands*

¶*Institute of Theoretical Physics, University of Regensburg, D-93050 Regensburg, Germany*

E-mail: korytar@karlov.mff.cuni.cz

S1 Review of symmetry properties of transport coefficients in molecular junctions

Principles of charge and spin transport in two-terminal devices were derived in the fields of nonequilibrium statistical mechanics and spintronics. Here we recollect some of them that are directly relevant for helical molecular junctions with SOC. **Principles 1** and **2** impose tight restrictions on the generation and detection of spin currents in nanoscale conductors. In **Principle 3** we show that TRI implies reciprocity relations between certain spin transport coefficients.

1

Principle 1: Absence of spin currents and spin filtering in single-channel non-magnetic junctions. We consider a strictly one-dimensional conductor with spin-orbit coupling. Assuming a single-particle scattering scenario, it can be shown that an unpolarized incident electron flux can not lead to polarized outgoing fluxes if the leads carry a single channel. This was shown by Kiselev and Kim[1] as a consequence of time-reversal invariance. Therefore, spin currents can not be induced by the voltage bias even in the non-linear regime, unless the above conditions are relaxed. The same negative statement applies to spin filtering.

Principle 2: Absence of chirality-induced linear magnetoconductance. Now let us consider attaching a ferromagnetic lead with magnetization M to the helix. The number of conduction channels can be arbitrary. Of interest is the difference between currents at reversed magnetizations: $I(M) - I(-M)$ (magnetocurrent) and the related difference in linear conductances, $G(M) - G(-M)$ (magnetoconductance).

A system with magnetization M and a current flowing has the property that the modulus of the current is invariant under time reversal, *i.e.* if one reverses the velocities of all particles and inverts the sign of M. A consequence of this invariance is the well-known Onsager's relation for the charge conductance,[2–4]

$$G(M) = G(-M). \tag{S1}$$

Note that the relation does not rely on the assumption of phase-coherence, unlike **Principle 1**. Furthermore, the relation also holds in presence of a magnetic field, if the latter is reversed along with M. It was recognized by Yang *et al.*[5] that Eq. (S1) prohibits the observation of spin filtering of chiral molecules in the linear response in the above mentioned setup. Nevertheless, magnetocurrent can be non-zero in the non-linear regime.

Onsager's theorem also precludes magnetoconductance in standard *ab-initio* transport calculations even in the non-linear response unless charge self-consistency with respect to the

bias voltage is achieved. We detail this argument in Section S1.1.

Principle 3: Reciprocity of spin-transport coefficients. Linear response relations shown in the main text involve charge and spin currents reacting to external voltage bias. In order to introduce reciprocity we need a slightly more general formulation that includes spin dependent chemical potentials. Following Nazarov and Blanter,[4] we introduce *spin accumulations* as differences in the respective chemical potentials between each spin species (in the same lead). Namely, the z-components of the spin accumulations are

$$W_z{}^{(\mathfrak{R})} = \left(\mu_\uparrow^{(\mathfrak{R})} - \mu_\downarrow^{(\mathfrak{R})} \right)/\hbar, \tag{S2a}$$

$$W_z{}^{(\mathfrak{L})} = \left(\mu_\uparrow^{(\mathfrak{L})} - \mu_\downarrow^{(\mathfrak{L})} \right)/\hbar. \tag{S2b}$$

Linear response of the currents to the voltage and spin accumulations is characterized by coefficients of the expansion

$$
\begin{aligned}
I(V, W_z{}^{(\mathfrak{R})}, W_z{}^{(\mathfrak{L})}) &= & GV &+& \widetilde{G}_z^{(\mathfrak{L})} W_z{}^{(\mathfrak{L})} &+& \widetilde{G}_z^{(\mathfrak{R})} W_z{}^{(\mathfrak{R})} &+ \ldots \\
I_z^{(\mathfrak{L})}(V, W_z{}^{(\mathfrak{R})}, W_z{}^{(\mathfrak{L})}) &= & G_z^{(\mathfrak{L})} V &+& G_{zz}^{(\mathfrak{L}\mathfrak{L})} W_z{}^{(\mathfrak{L})} &+& G_{zz}^{(\mathfrak{L}\mathfrak{R})} W_z{}^{(\mathfrak{R})} &+ \ldots \\
I_z^{(\mathfrak{R})}(V, W_z{}^{(\mathfrak{R})}, W_z{}^{(\mathfrak{L})}) &= & G_z^{(\mathfrak{R})} V &+& G_{zz}^{(\mathfrak{R}\mathfrak{L})} W_z{}^{(\mathfrak{L})} &+& G_{zz}^{(\mathfrak{R}\mathfrak{R})} W_z{}^{(\mathfrak{R})} &+ \ldots,
\end{aligned}
\tag{S3}
$$

where we suppressed terms of higher order. Naturally, additional measurements of spin in other directions than z would bring up coefficients in these directions, too, but they are of no relevance for the present work. See Ref.[6] for a general formulation. Time-reversal invariance implies the reciprocities[6]

$$G_z^{(\mathfrak{R})} = +\widetilde{G}_z^{(\mathfrak{R})} \tag{S4a}$$

$$G_z^{(\mathfrak{L})} = -\widetilde{G}_z^{(\mathfrak{L})} \tag{S4b}$$

$$G_{zz}^{(\mathfrak{L}\mathfrak{R})} = -G_{zz}^{(\mathfrak{R}\mathfrak{L})}. \tag{S4c}$$

3

We remark that the difference in signs of the right-hand sides above results from our definition of the currents that measure particles entering the junction through the left contact, or, leaving the junction through the right contact.

In molecular junctions, these relations offer an alternative way to measure the spin currents in linear response. Namely, the $\mathfrak{L}$ and $\mathfrak{R}$ spin currents induced by a finite V but zero $W_z^{(\mathfrak{R}/\mathfrak{L})}$ are identical, up to a sign, to the charge current that results from the spin accumulation in the $\mathfrak{L}$ and $\mathfrak{R}$ leads, respectively, at $V = 0$. The practical application of the above identity is limitted by the ability to strictly separate bias drop from spin accumulations. Further reciprocities emerge with the measurement of heat currents and temperature differences; see Ref.[6] for a review.

We re-derive explicit expressions for the transport coefficients in Landauer formalism in Section S5 of this Supplementary Information. In Section S4 we review various symmetry properties of the scattering operator that apply to the Michaeli-Naaman model and employ them to derive cross-relations between spin conductances in Sec. S5, including Onsager relations. Explicit evaluation of the scattering operator for the model is detailed in Sections S2, S3.

S1.1 Absence of chirality-induced magnetocurrent in common *ab-initio* transport calculations

The state-of-the-art *ab-initio* method employs the Landauer formalism extended to non-equilibrium. It assumes quantum coherence, effective single-particle states and thermodynamic equilibrium in each lead. The electric current is given by the formula

$$I(V, M) = \frac{e}{h} \int \left[n_{\mathrm{F}}\left(E - \mu_{\mathfrak{L}}(V) \right) - n_{\mathrm{F}}\left(E - \mu_{\mathfrak{R}}(V) \right) \right] \sum_{\sigma\sigma'} T_{\sigma\sigma'}(E, V, M) \, \mathrm{d}E \,. \qquad (S5)$$

The central quantity in the above equation is the spin-resolved transmission probability $T_{\sigma\sigma'}(E, V, M)$. We explicitly indicate its dependence on the voltage V and a static mag-

netization of the junction M.[i] The $T_{\sigma\sigma'}(E, V, M)$ results from a quantum-mechanical calculation, *e.g.*, by the non-equilibrium Green's function technique. The remaining factor in the integrand contains the voltage-dependent energy window allowed by the Pauli principle. The Fermi-Dirac distribution n_{F} depends explicitly on the chemical potential of each lead, $\mu_{\mathfrak{L}/\mathfrak{R}}(V)$. The boundary condition $\mu_{\mathfrak{L}}(V) - \mu_{\mathfrak{R}}(V) = eV$ is imposed by the external bias voltage V. In this discussion we suppress the temperature dependence and assume that both leads have equal temperatures.

The *ab-initio* calculations based on density-functional theory deliver both $\mu_{\mathfrak{R}/\mathfrak{L}}(V)$ and $T_{\sigma\sigma'}(E, V, M)$ from the Kohn-Sham system. An explicit calculation of the voltage dependencies in the previous formulæ is rarely performed. A frequently employed approximation

$$T_{\sigma\sigma'}(E, V, M) \approx T_{\sigma\sigma'}(E, 0, M) \tag{S6}$$

when plugged into Eq. (S5), still delivers a non-linear IV curve.

Time-reversal invariance implies the following symmetry property of the transmission probability[6]

$$\sum_{\sigma\sigma'} T_{\sigma\sigma'}(E, 0, M) = \sum_{\sigma\sigma'} T_{\sigma\sigma'}(E, 0, -M). \tag{S7}$$

It follows trivially that the magnetocurrent $I(V, M) - I(V, -M)$ vanishes when the approximation (S6) is used. We conclude that the common *ab-initio* methodology can not describe chirality-induced nonlinear magnetocurrent due to Onsager's theorem.

---

[i]The scattering probabilities are further differentiated according to the direction of flow, *i.e.* from left to right or *vice versa*; see the analysis of the scattering matrix of the helical model in the Supplementary Information. Both directions of flow yield the same *charge current* and therefore we suppress the direction of flow in the notation of $T_{\sigma\sigma'}$.

S2 Spectrum and eigenstates of a helical tube

The Hamiltonian, Eq. (10) of the main text, can be rewritten as

$$\hat{h}_m(k) = \left(\frac{1}{2} + \frac{1}{2}k^2\right)\hat{\sigma}_0 + \lambda\mathfrak{b}\cdot\boldsymbol{\sigma} \tag{S8}$$

where the first term on the right side is proportional to the unit matrix $\hat{\sigma}_0$; $\boldsymbol{\sigma}$ abbreviates the Pauli-matrices and $\mathfrak{b} = (b_x, b_y, b_z) = (0, -\tilde{\kappa}m, -k)$.

The second term has eigenvalues

$$\lambda k \xi_\alpha, \quad \text{where } \xi_\alpha = \alpha\sqrt{1 + \left(\frac{\tilde{\kappa}m}{k}\right)^2} \text{ for } \alpha = \pm 1.$$

The eigenvectors read

$$\Psi_{m\alpha}(k) = \frac{\lambda}{\sqrt{k^2 + \left(\frac{\tilde{\kappa}m}{1+\xi_\alpha}\right)^2}}\begin{pmatrix} \mathrm{i}\frac{\tilde{\kappa}m}{(1+\xi_\alpha)} \\ k \end{pmatrix}. \tag{S9}$$

We chose the sign of the eigenvalue, $\alpha\lambda\cdot\text{sgn}(k)$, and the phase of the eigenspinors such that for $k \to \pm\infty$ or $\tilde{\kappa} \to 0$ the eigenstates approach up, down spinors, $\alpha = \sigma$. The eigenenergies of the Hamiltonian are

$$E_{m,\alpha}(k) = \frac{1}{2}(k + \lambda\xi_\alpha)^2 - \frac{1}{2}\left(\frac{\tilde{\kappa}m}{k}\right)^2 \tag{S10}$$

For small $\tilde{\kappa}$, it resembles the spectrum of the straight tube, except that there is a gap $E \in (\frac{1}{2} - |\tilde{\kappa}m|, \frac{1}{2} + |\tilde{\kappa}m|)$ around $k = 0$. The inverse dispersion reads

$$k_{m\alpha\beta} = \zeta\lambda\alpha\sqrt{2\left[E + \frac{1}{2} + \beta\sqrt{2E + \tilde{\kappa}^2m^2}\right]} \tag{S11}$$

$$\zeta = \left[\text{sgn}\left(E - \frac{1}{2}\right)\right]^{\frac{(1-\beta)}{2}} \tag{S12}$$

and it is labeled by the branch β for each eigenstate α.

Real energies of evanescent modes and their eigenspinors can be obtained by analytic continuation of the expressions into the complex k-domain. The dispersion of the evanescent modes is shown in Fig. S1. The expectation value of $\hat{\sigma}_z$ is zero in these states. An inspection shows that their spin vector rotates in the xy-plane.
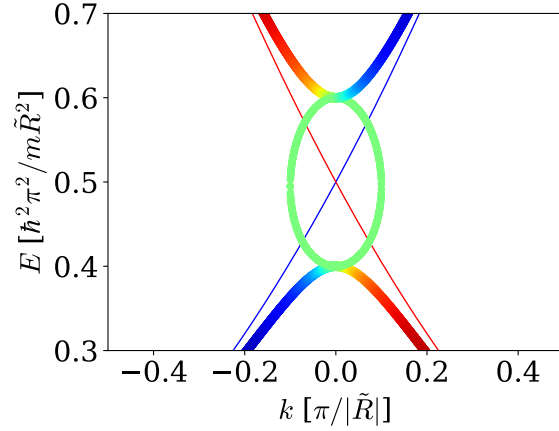

Figure S1: Dispersion of the helix in the region of the spin-orbit gap. The parameters and the symbols are identical to the Fig. 3 of the main text. Additionally, we plot the energies of the evanescent states within the gap (smaller dots).

S3 Evaluation of the scattering matrix of the helical junction

Expressions for the scattering wavefunctions are derived in this section by matching the current operator on both sides of the interfaces. The wave function coefficients deliver scattering matrix elements straightforwardly. Throughout the following sections we employ dimensionless energies and lengths introduced in the main text but drop the primes from the notation.

Probability current. In the gauged Hilbert's space the time evolution is generated by the Hamiltonian Eq. (9) of the main text. From the continuity equation of a probability density it is possible to derive an explicit form of the probability current

$$j(s,t) = \frac{1}{2}\left\{ \Psi^\dagger \left(-\mathrm{i}\partial_s + \tilde{\gamma}m - \lambda\hat{\sigma}_z\right)\Psi + [\left(-\mathrm{i}\partial_s + \tilde{\gamma}m - \lambda\hat{\sigma}_z\right)\Psi]^\dagger \Psi \right\} \tag{S13}$$

The form of the current operator is analogous to the one in the problem of an electron in a magnetic field, except that the gauge potential is matrix-valued (non-Abelian).

The above expression for the current operates on the gauged wavefunctions in the helix. Upon employing the inverse gauge transformation $\Psi' = e^{-\mathrm{i}s\lambda\hat{\sigma}_z}\Psi$ in Eq. (S13), we obtain an expression

$$j'(s,t) = \frac{1}{2}\left\{ \Psi'^\dagger \left(-\mathrm{i}\partial_s + \tilde{\gamma}m\right)\Psi' + [\left(-\mathrm{i}\partial_s + \tilde{\gamma}m\right)\Psi']^\dagger \Psi' \right\} \tag{S14}$$

where primes indicate ungauged expressions. In the straight tubes, the current is given by the above expression with $\tilde{\gamma} = 0$.

Furthermore, the Abelian gauge potential $\tilde{\gamma}m$ can be removed from the Hamiltonian by the gauge transformation $e^{\mathrm{i}s\tilde{\gamma}m}$ in the Hilber's space of the molecule. Correspondingly, $\tilde{\gamma}$ will vanish from the current operator. As a corollary, the expectation values of the (spin) current dentisty in Hamiltonian eigenstates are $\tilde{\gamma}$ independent. Hence, when leads are attached,

scattering probabilities will be likewise $\tilde{\gamma}$ independent, although the scattering phases won't. It is known that in one dimension, a vector potential does not have physically observable effects. Therefore we set $\tilde{\gamma} = 0$ in what follows.

Scattering wavefunctions. The scattering picture is most transparent in the ungauged Hilbert's space. There, the wavefunctions in the leads are incoming and outgoing planewaves with wavenumbers $\pm\sqrt{2E}$. In the helix, we apply the inverse gauge transformation $e^{-i\lambda\hat{\sigma}_z s}$ to the eigenvectors, Eq. (S9).

We consider a helix of length L connected to straight semi-infinite tubes. First, a spin-up electron is coming from the left tube with energy $E > 0$. In the left tube the wavefunction reads

$$\psi_m^E(s) = \begin{pmatrix} 1 \\ 0 \end{pmatrix} e^{iqs} + \begin{pmatrix} r_{\uparrow\uparrow} \\ r_{\downarrow\uparrow} \end{pmatrix} e^{-iqs}, \quad s < 0, \quad q = \sqrt{2E}. \tag{S15}$$

The first term represents an incident electron and the second term represents a reflected electron, with reflection amplitudes $r_{\sigma\sigma'}$, where the left (right) index labels the final (initial) state.

In the right lead $(s > L)$, the transmitted wavefunction reads

$$\psi_m^E(s) = \begin{pmatrix} t_{\uparrow\uparrow} \\ t_{\downarrow\uparrow} \end{pmatrix} e^{iqs}. \tag{S16}$$

Similarly, for an incoming down electron the following relations hold

$$\psi_m^E(s) = \begin{pmatrix} 0 \\ 1 \end{pmatrix} e^{iqs} + \begin{pmatrix} r_{\uparrow\downarrow} \\ r_{\downarrow\downarrow} \end{pmatrix} e^{-iqs}, \quad s < 0 \tag{S17}$$

$$\psi_m^E(s) = \begin{pmatrix} t_{\uparrow\downarrow} \\ t_{\downarrow\downarrow} \end{pmatrix} e^{iqs}, \quad s > L. \tag{S18}$$

In the central (helical) region, the form of the wavefunction depends on whether we are in

9

the gap region or away from it. It consists always from four eigenstates, with amplitudes a, b, c, d. Away from the gap, the wavefunction contains planewaves only,

$$\psi_m^E(s) = a\, e^{i(k_{m++}-\lambda\hat{\sigma}_z)s} \cdot \Psi_{m,+}(k_{m++}) \tag{S19}$$

$$+ b\, e^{i(k_{m-+}-\lambda\hat{\sigma}_z)s} \cdot \Psi_{m,-}(k_{m-+}) \tag{S20}$$

$$+ c\, e^{i(k_{m+-}-\lambda\hat{\sigma}_z)s} \cdot \Psi_{m,+}(k_{m+-}) \tag{S21}$$

$$+ d\, e^{i(k_{m--}-\lambda\hat{\sigma}_z)s} \cdot \Psi_{m,-}(k_{m--}), \quad 0 < s < L \tag{S22}$$

where the wavenumber corresponding to E is given in the Eq. (S11). In the gap region, two modes become evanescent and the above expression has to be analytically continued. Because of the inverse gauge transformation operator, each component of the spinors has a distinct spatial dependence.

The coefficients a, b, c, d (for a given incoming spin) and the transmission and reflection amplitudes are determined by matching the expectation values of the probability current at both interfaces.

Wavefunction matching. Let $\psi_m^E(s)$ be the scattering wavefunction as given in previous sections. The current must be continuous at the interfaces. Employing the expression (S14), the conditions are

$$\psi_m^E(0+) = \psi_m^E(0-) \tag{S23a}$$

$$-i\partial_s\psi_m^E(0+) = -i\partial_s\psi_m^E(0-) \tag{S23b}$$

$$\psi_m^E(L-) = \psi_m^E(L+) \tag{S23c}$$

$$-i\partial_s\psi_m^E(L-) = -i\partial_s\psi_m^E(L+) \tag{S23d}$$

For a given direction of the incoming spin, the wavefunction contains 8 unknown coefficients, which can be completely determined by the Eq. (S23).

In presence of a delta barrier at the left contact $(s = 0)$, the Hamiltonian gains the potential term

$$v(s) = c\delta(s) \cdot \hat{\sigma}_0.$$

The matching condition for the left contact becomes

$$\psi_m^E(0+) = \psi_m^E(0-) \tag{S24}$$

$$-\mathrm{i}\partial_s\psi_m^E(0+) = -\mathrm{i}\partial_s\psi_m^E(0-) - \mathrm{i}2c\,\psi_m^E(0). \tag{S25}$$

Scattering probabilities. Fig. S2 shows the left and right transmission and reflection probabilities for a helix with 6 turns and the same parameters as in Fig. 3.
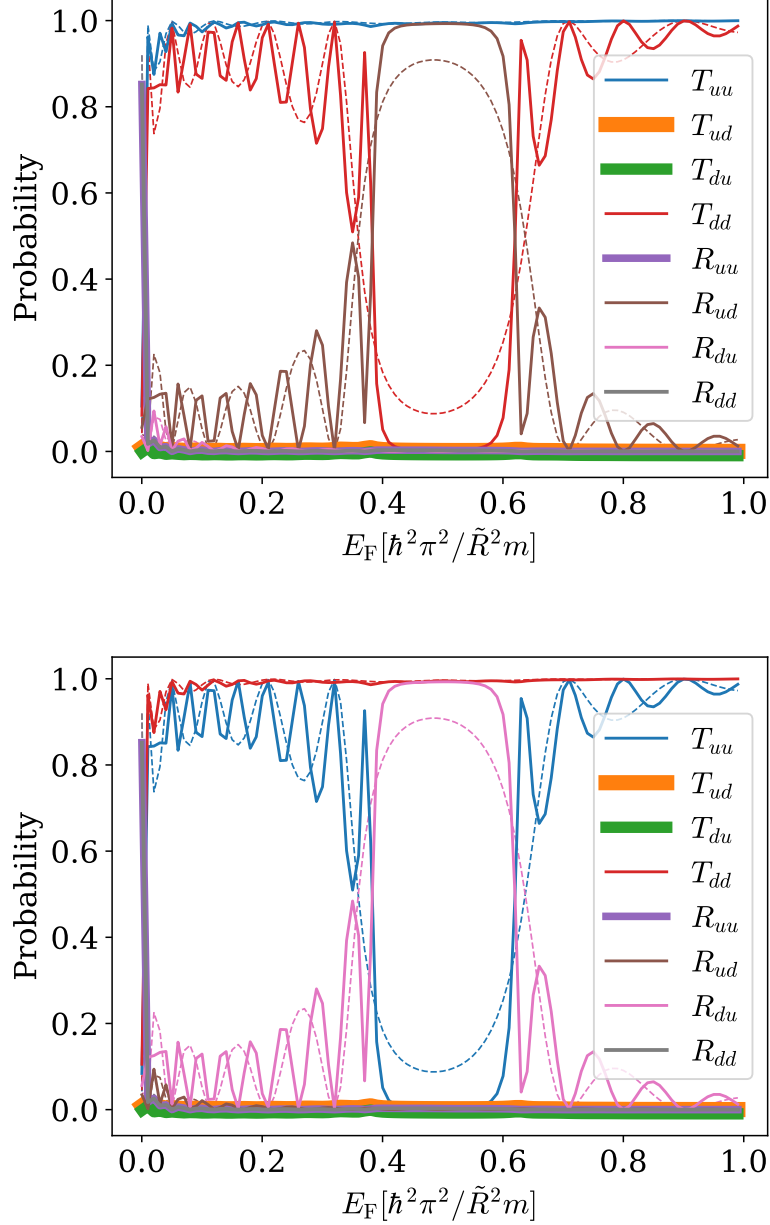
Figure S2: Scattering probabilities for transmission and reflection from the **left** (top panel) and **right** (bottom) leads, (u)p and (d)own spins. The probabilities are m-independent for $m = \pm 1$. Parameters: $\tilde{\kappa} = 0.1, \lambda = -1$, same as in Fig. 3 of the main text, and the helix has 6 (solid lines) and 3 (dashed lines) turns. $E = 0, 0.4, 0.6$ mark the bottom of the conduction band of the lead, and the limits of the gap of the helical bandstructure.

S4 Symmetries of the scattering matrix

We assume a scattering problem, defined by the scattering Hamiltonian

$$\hat{H}_m(s) = \frac{1}{2}\left(-\mathrm{i}\frac{\mathrm{d}}{\mathrm{d}s} - \lambda\hat{\sigma}_z\right)^2 - \lambda\tilde{\kappa}(s)m\hat{\sigma}_y, \tag{S26}$$

where $\tilde{\kappa}(s) = \tilde{\kappa}$ for $-L/2 < s < L/2$ (central region) and zero in the left lead ($s < -L/2$) and the right lead ($s > L/2$). In what follows we shall make use of the basic invariance properties of $\hat{H}_m(s)$ in order to derive symmetry relations of the scattering matrix. These invariance properties may hold true under more general conditions for a wider class of Hamiltonians. For example, the contacts may be modeled by a continuous decrease of $\tilde{\kappa}(s)$, or the contacts could model vacuum tunneling. We start our exposure with charge conservation (implying the well known unitarity), follow with time-reversal and end up with spatial inversions.

S4.1 Notation

The leads ($\tilde{\kappa}(s) = 0$) represent "straight tubes" and conserve both $\hat{\sigma}_z$ and the orbital angular momentum m. On the other hand, in the central region $-L/2 < s < L/2$ only m is conserved. An incoming wave in the left lead at energy E with spin $\uparrow$ in the channel m is denoted by $\left|\Phi_{E,\uparrow,m}^{(\mathrm{In},\mathfrak{L})}\right\rangle$. Similarly, an incoming wave in the right lead with the same quantum numbers is denoted by $\left|\Phi_{E,\uparrow,m}^{(\mathrm{In},\mathfrak{R})}\right\rangle$. Since the scattering processes conserve E and m, for a fixed m we can write a general incoming wave as a 4-vector,

$$\left|\Phi_{E,m}^{(\mathrm{In})}\right\rangle = \left(\left|\Phi_{E,\uparrow,m}^{(\mathrm{In},\mathfrak{L})}\right\rangle, \left|\Phi_{E,\downarrow,m}^{(\mathrm{In},\mathfrak{L})}\right\rangle, \left|\Phi_{E,\uparrow,m}^{(\mathrm{In},\mathfrak{R})}\right\rangle, \left|\Phi_{E,\downarrow,m}^{(\mathrm{In},\mathfrak{R})}\right\rangle\right)^{\mathrm{T}}. \tag{S27}$$

The scattering operator $\hat{S}_m(E)$ maps $\left|\Phi_{E,m}^{(\mathrm{In})}\right\rangle$ into an outgoing wave $\left|\Phi_{E,m}^{(\mathrm{Out})}\right\rangle$,

$$\left|\Phi_{E,m}^{(\mathrm{Out})}\right\rangle = \hat{S}_m(E)\left|\Phi_{E,m}^{(\mathrm{In})}\right\rangle, \tag{S28}$$

13

where

$$\left| \Phi_{E,m}^{(\text{Out})} \right\rangle = \left(\left| \Phi_{E,\uparrow,m}^{(\text{Out},\mathcal{L})} \right\rangle, \left| \Phi_{E,\downarrow,m}^{(\text{Out},\mathcal{L})} \right\rangle, \left| \Phi_{E,\uparrow,m}^{(\text{Out},\mathcal{R})} \right\rangle, \left| \Phi_{E,\downarrow,m}^{(\text{Out},\mathcal{R})} \right\rangle \right)^{\text{T}}. \tag{S29}$$

From now on we suppress the energy dependence in the notation; we denote the matrix elements of $\hat{S}_m$ in this basis set by

$$\hat{S}_m \equiv \begin{pmatrix} r_{\uparrow\uparrow,m}^{(\mathcal{L}\mathcal{L})} & r_{\uparrow\downarrow,m}^{(\mathcal{L}\mathcal{L})} & t_{\uparrow\uparrow,m}^{(\mathcal{L}\mathcal{R})} & t_{\uparrow\downarrow,m}^{(\mathcal{L}\mathcal{R})} \\[2mm] r_{\downarrow\uparrow,m}^{(\mathcal{L}\mathcal{L})} & r_{\downarrow\downarrow,m}^{(\mathcal{L}\mathcal{L})} & t_{\downarrow\uparrow,m}^{(\mathcal{L}\mathcal{R})} & t_{\downarrow\downarrow,m}^{(\mathcal{L}\mathcal{R})} \\[2mm] t_{\uparrow\uparrow,m}^{(\mathcal{R}\mathcal{L})} & t_{\uparrow\downarrow,m}^{(\mathcal{R}\mathcal{L})} & r_{\uparrow\uparrow,m}^{(\mathcal{R}\mathcal{R})} & r_{\uparrow\downarrow,m}^{(\mathcal{R}\mathcal{R})} \\[2mm] t_{\downarrow\uparrow,m}^{(\mathcal{R}\mathcal{L})} & t_{\downarrow\downarrow,m}^{(\mathcal{R}\mathcal{L})} & r_{\downarrow\uparrow,m}^{(\mathcal{R}\mathcal{R})} & r_{\downarrow\downarrow,m}^{(\mathcal{R}\mathcal{R})} \end{pmatrix} \equiv \begin{pmatrix} r_{\sigma\sigma',m}^{(\mathcal{L}\mathcal{L})} & t_{\sigma\sigma',m}^{(\mathcal{L}\mathcal{R})} \\[3mm] t_{\sigma\sigma',m}^{(\mathcal{R}\mathcal{L})} & r_{\sigma\sigma',m}^{(\mathcal{R}\mathcal{R})} \end{pmatrix} \tag{S30}$$

S4.2 Unitarity from the charge conservation

Each matrix element of (S30), when squared, gives a scattering probability. We shall use capital letters for the probabilities, for instance, $|t_{\uparrow\uparrow,m}^{(\mathcal{R}\mathcal{L})}|^2 = T_{\uparrow\uparrow,m}^{(\mathcal{R}\mathcal{L})}$. For reference, we reproduce here some consequences of unitarity of the scattering matrix:

$$1 = \sum_{\sigma} R_{\sigma\sigma',m}^{(\mathcal{L}\mathcal{L})} + T_{\sigma\sigma',m}^{(\mathcal{R}\mathcal{L})} \tag{S31a}$$

$$1 = \sum_{\sigma} R_{\sigma\sigma',m}^{(\mathcal{R}\mathcal{R})} + T_{\sigma\sigma',m}^{(\mathcal{L}\mathcal{R})} \tag{S31b}$$

$$1 = \sum_{\sigma'} R_{\sigma\sigma',m}^{(\mathcal{L}\mathcal{L})} + T_{\sigma\sigma',m}^{(\mathcal{L}\mathcal{R})} \tag{S31c}$$

$$1 = \sum_{\sigma'} R_{\sigma\sigma',m}^{(\mathcal{R}\mathcal{R})} + T_{\sigma\sigma',m}^{(\mathcal{R}\mathcal{L})} \tag{S31d}$$

The first two equations state that the incoming flux must be distributed in a conserving way into the outgoing fluxes. The last two equations require normalization of the outgoing

14

waves.

We shall make frequent use of an auxiliary identity obtained by multiplying the Eqs. (S31c,S31d) by σ and summing,

$$\sum_{\sigma\sigma'} \sigma T^{(\mathfrak{LR})}_{\sigma\sigma',m} = -\sum_{\sigma\sigma'} \sigma R^{(\mathfrak{LL})}_{\sigma\sigma',m}, \tag{S32a}$$

$$\sum_{\sigma\sigma'} \sigma T^{(\mathfrak{RL})}_{\sigma\sigma',m} = -\sum_{\sigma\sigma'} \sigma R^{(\mathfrak{RR})}_{\sigma\sigma',m} \tag{S32b}$$

S4.3   Time-reversal invariance

The condition of time reversal invariance imposes the following restriction on the matrix elements:

$$\left\langle \Phi^{(\text{Out})}_m \right| \hat{S}_m \left| \Phi^{(\text{In})}_m \right\rangle = \left\langle T\Phi^{(\text{In})}_m \right| \hat{S}_m \left| T\Phi^{(\text{Out})}_m \right\rangle \tag{S33}$$

$T = -\mathrm{i}\hat{\sigma}_y K$ is the time reversal operator; its effect on the In and Out waves amounts to

$$\left| T\Phi^{(\text{In})}_m \right\rangle = \left(\left| \Phi^{(\text{Out},\mathfrak{L})}_{E,\downarrow,-m} \right\rangle, -\left| \Phi^{(\text{Out},\mathfrak{L})}_{E,\uparrow,-m} \right\rangle, \left| \Phi^{(\text{Out},\mathfrak{R})}_{E,\downarrow,-m} \right\rangle, -\left| \Phi^{(\text{Out},\mathfrak{R})}_{E,\uparrow,-m} \right\rangle \right)^{\mathrm{T}} \tag{S34}$$

$$\left| T\Phi^{(\text{Out})}_m \right\rangle = \left(\left| \Phi^{(\text{In},\mathfrak{L})}_{E,\downarrow,-m} \right\rangle, -\left| \Phi^{(\text{In},\mathfrak{L})}_{E,\uparrow,-m} \right\rangle, \left| \Phi^{(\text{In},\mathfrak{R})}_{E,\downarrow,-m} \right\rangle, -\left| \Phi^{(\text{In},\mathfrak{R})}_{E,\uparrow,-m} \right\rangle \right)^{\mathrm{T}}. \tag{S35}$$

Notice that the minus sign is specific to the transformation of spinors. The following cross-relationships between matrix elements are implied,

$$r^{(\mathfrak{LL})}_{\sigma,\sigma',m} = (\sigma\sigma')\, r^{(\mathfrak{LL})}_{-\sigma',-\sigma,-m}, \qquad\qquad R^{(\mathfrak{LL})}_{\uparrow\uparrow,m} = R^{(\mathfrak{LL})}_{\downarrow\downarrow,-m} \tag{S36a}$$

$$r^{(\mathfrak{RR})}_{\sigma,\sigma',m} = (\sigma\sigma')\, r^{(\mathfrak{RR})}_{-\sigma',-\sigma,-m}, \qquad\qquad R^{(\mathfrak{RR})}_{\uparrow\uparrow,m} = R^{(\mathfrak{RR})}_{\downarrow\downarrow,-m}, \tag{S36b}$$

$$t^{(\mathfrak{LR})}_{\sigma,\sigma',m} = (\sigma\sigma')\, t^{(\mathfrak{RL})}_{-\sigma',-\sigma,-m}, \qquad\qquad T^{(\mathfrak{LR})}_{\sigma,\sigma',m} = T^{(\mathfrak{RL})}_{-\sigma',-\sigma,-m}. \tag{S36c}$$

The above formulæ have important consequences for the occurrence of spin polarization. Consider an unpolarized incident flux in the left lead. The spin conserving reflection processes

15

are balanced due to Eq. (S36a). If spin polarization results from the reflection, it must be due to spin flipping processes.[5]

If we set $m = 0$ in the Eq. (S36) we restrict to the single channel. Very strict conditions follow for the reflection amplitudes,

$$r^{(\mathfrak{LL})}_{\sigma\sigma} = r^{(\mathfrak{LL})}_{-\sigma,-\sigma}, \qquad\qquad\qquad r^{(\mathfrak{RR})}_{\sigma\sigma} = r^{(\mathfrak{RR})}_{-\sigma,-\sigma} \qquad\qquad (S37)$$

$$r^{(\mathfrak{LL})}_{\downarrow\uparrow} = r^{(\mathfrak{LL})}_{\uparrow\downarrow} = 0, \qquad\qquad\qquad r^{(\mathfrak{RR})}_{\downarrow\uparrow} = r^{(\mathfrak{RR})}_{\uparrow\downarrow} = 0. \qquad\qquad (S38)$$

When combined with unitarity, these relations prohibit spin filtering in single channel wires, as proven by Kiselev and Kim.[1]

S4.4   Spatial symmetries

Here we explore the consequences of various operations on the spatial (spin and orbital) degrees of freedom.

The basic algebraic identities $[\hat{\sigma}_z]^3 = \hat{\sigma}_z$ and $\hat{\sigma}_z\hat{\sigma}_y\hat{\sigma}_z = -\hat{\sigma}_y$ can be combined to yield the following invariance property

$$\hat{\sigma}_z \hat{H}_m(s) \hat{\sigma}_z = \hat{H}_{-m}(s) \qquad\qquad (S39)$$

where $\hat{H}_m(s)$ is introduced in the Eq. (S26).[ii]. The above relation holds for both the straight tube and the helix. Therefore, the scattering matrix obeys

$$\hat{\sigma}_z \hat{S}_{-m} \hat{\sigma}_z = \hat{S}_m \qquad\qquad (S40)$$

[ii]We remind that the operator $\hat{\sigma}_z = \mathrm{i}\exp(-\mathrm{i}\hat{\sigma}_z\pi/2)$ performs a rotation by π around the z axis of the spin degrees of freedom (up to a phase factor); it effectively inverts the sign of $\hat{\sigma}_y$. Such rotation can be compensated for by flipping the sign of m.

i.e.

$$r^{(\mathcal{LL})}_{\sigma,\sigma',m} = (\sigma\sigma')\, r^{(\mathcal{LL})}_{\sigma,\sigma',-m}, \qquad\qquad R^{(\mathcal{LL})}_{\sigma,\sigma',m} = R^{(\mathcal{LL})}_{\sigma,\sigma',-m}, \tag{S41a}$$

$$r^{(\mathfrak{RR})}_{\sigma,\sigma',m} = (\sigma\sigma')\, r^{(\mathfrak{RR})}_{\sigma,\sigma',-m}, \qquad\qquad R^{(\mathfrak{RR})}_{\sigma,\sigma',m} = R^{(\mathfrak{RR})}_{\sigma,\sigma',-m} \tag{S41b}$$

$$t^{(\mathcal{LR})}_{\sigma,\sigma',m} = (\sigma\sigma')\, t^{(\mathcal{LR})}_{\sigma,\sigma',-m}, \qquad\qquad T^{(\mathcal{LR})}_{\sigma,\sigma',m} = T^{(\mathcal{LR})}_{\sigma,\sigma',-m} \tag{S41c}$$

$$t^{(\mathfrak{RL})}_{\sigma,\sigma',m} = (\sigma\sigma')\, t^{(\mathfrak{RL})}_{\sigma,\sigma',-m}, \qquad\qquad T^{(\mathfrak{RL})}_{\sigma,\sigma',m} = T^{(\mathfrak{RL})}_{\sigma,\sigma',-m}. \tag{S41d}$$

Clearly, all scattering probabilities are m-independent.

Combining the latter symmetry with time-reversal yields identities equating elements of the scattering matrix from the same m sector, as can be derived using Eqs. (S41,S36):

$$r^{(\mathcal{LL})}_{\sigma,\sigma',m} = r^{(\mathcal{LL})}_{-\sigma',-\sigma,m}, \qquad\qquad R^{(\mathcal{LL})}_{\uparrow\uparrow,m} = R^{(\mathcal{LL})}_{\downarrow\downarrow,m} \tag{S42a}$$

$$r^{(\mathfrak{RR})}_{\sigma,\sigma',m} = r^{(\mathfrak{RR})}_{-\sigma',-\sigma,m}, \qquad\qquad R^{(\mathfrak{RR})}_{\uparrow\uparrow,m} = R^{(\mathfrak{RR})}_{\downarrow\downarrow,m} \tag{S42b}$$

$$t^{(\mathcal{LR})}_{\sigma,\sigma',m} = t^{(\mathfrak{RL})}_{-\sigma',-\sigma,m}, \qquad\qquad T^{(\mathcal{LR})}_{\sigma,\sigma',m} = T^{(\mathfrak{RL})}_{-\sigma',-\sigma,m}. \tag{S42c}$$

S4.4.1   Parity

The helicity of the helix is invariant under inversion of all three spatial coordinates. Such an operation reverses the left and right leads, though. We exploit this property in what follows. The Hamiltonian is not invariant under s-reversal $\hat{P}_s : s \mapsto -s$, but under the joint operation of $\hat{P}_s$ and $\hat{\sigma}_y$,[7]

$$\left(\hat{\sigma}_y \hat{P}_s\right) \hat{H}_m(s) \left(\hat{P}_s \hat{\sigma}_y\right) = \hat{H}_m(s), \tag{S43}$$

and so is $\hat{S}_m$. Consequently,

$$r^{(\mathcal{LL})}_{\sigma,\sigma',m} = (\sigma\sigma')\, r^{(\mathfrak{RR})}_{-\sigma,-\sigma',m}, \qquad\qquad R^{(\mathcal{LL})}_{\sigma,\sigma',m} = R^{(\mathfrak{RR})}_{-\sigma,-\sigma',m}, \tag{S44a}$$

$$t^{(\mathcal{LR})}_{\sigma,\sigma',m} = (\sigma\sigma')\, t^{(\mathfrak{RL})}_{-\sigma,-\sigma',m}, \qquad\qquad T^{(\mathcal{LR})}_{\sigma,\sigma',m} = T^{(\mathfrak{RL})}_{-\sigma,-\sigma',m}, \tag{S44b}$$

where we used the fact that $\hat{P}_s$ interchanges the leads. Combining parity and time reversal

17

yields $T^{(\mathfrak{L}\mathfrak{R})}_{\uparrow\downarrow,m} = T^{(\mathfrak{L}\mathfrak{R})}_{\downarrow\uparrow,m}$ and $T^{(\mathfrak{R}\mathfrak{L})}_{\uparrow\downarrow,m} = T^{(\mathfrak{R}\mathfrak{L})}_{\downarrow\uparrow,m}$.

S4.4.2   Remark: Structure of the probability matrix

The spatiotemporal invariance properties can be used to lay out the structure of the matrix of scattering probabilities, using 6 independent parameters only,

$$
\begin{pmatrix}
R^{(\mathfrak{L}\mathfrak{L})}_{\uparrow\uparrow,m} & R^{(\mathfrak{L}\mathfrak{L})}_{\uparrow\downarrow,m} & T^{(\mathfrak{L}\mathfrak{R})}_{\uparrow\uparrow,m} & T^{(\mathfrak{L}\mathfrak{R})}_{\uparrow\downarrow,m} \\[2mm]
R^{(\mathfrak{L}\mathfrak{L})}_{\downarrow\uparrow,m} & R^{(\mathfrak{L}\mathfrak{L})}_{\downarrow\downarrow,m} & T^{(\mathfrak{L}\mathfrak{R})}_{\downarrow\uparrow,m} & T^{(\mathfrak{L}\mathfrak{R})}_{\downarrow\downarrow,m} \\[2mm]
T^{(\mathfrak{R}\mathfrak{L})}_{\uparrow\uparrow,m} & T^{(\mathfrak{R}\mathfrak{L})}_{\uparrow\downarrow,m} & R^{(\mathfrak{R}\mathfrak{R})}_{\uparrow\uparrow,m} & R^{(\mathfrak{R}\mathfrak{R})}_{\uparrow\downarrow,m} \\[2mm]
T^{(\mathfrak{R}\mathfrak{L})}_{\downarrow\uparrow,m} & T^{(\mathfrak{R}\mathfrak{L})}_{\downarrow\downarrow,m} & R^{(\mathfrak{R}\mathfrak{R})}_{\downarrow\uparrow,m} & R^{(\mathfrak{R}\mathfrak{R})}_{\downarrow\downarrow,m}
\end{pmatrix}
=
\begin{pmatrix}
a & b & c & d \\
g & a & d & f \\
f & d & a & g \\
d & c & b & a
\end{pmatrix},
\quad \text{independent of } m. \tag{S45}
$$

We can recognize immediately that the symmetries of the scattering Hamiltonian allow for spin polarization due to spin-flipping reflections and non-flipping transmissions. Specifically, spin polarization is generated if the expressions

$$
R^{(\mathfrak{R}\mathfrak{R})}_{\downarrow\uparrow,m} - R^{(\mathfrak{R}\mathfrak{R})}_{\uparrow\downarrow,m}, \; T^{(\mathfrak{R}\mathfrak{L})}_{\uparrow\uparrow,m} - T^{(\mathfrak{R}\mathfrak{L})}_{\downarrow\downarrow,m}, \quad \text{and with } \mathfrak{R} \longleftrightarrow \mathfrak{L}
$$

are non-zero. Other spin processes are balanced and do not contribute to the polarization.

S5   Transport coefficients in the Landauer formalism and their symmetry relations

We derive explicit expression for the transport coefficients, Eq. (S3), in Landauer formalism, employing the properties of the scattering probability matrix that we have given in the previous section.

S5.1   Expressions for the currents

Charge current in the left lead is simply given by summing (a) an incident flux in the left lead, (b) a back-reflected flux in the left lead and (c) the fluxes transmitted from the right lead, namely,

$$I^{(\mathfrak{L})} = \frac{e}{h} \sum_m \sum_{\sigma'} \int \mathrm{d}E \left\{ n_\mathrm{F}(E - \mu_\mathfrak{L}^{\sigma'}) \left[1 - \sum_\sigma R_{\sigma\sigma',m}^{(\mathfrak{L}\mathfrak{L})} \right] - n_\mathrm{F}(E - \mu_\mathfrak{R}^{\sigma'}) \sum_\sigma T_{\sigma\sigma',m}^{(\mathfrak{L}\mathfrak{R})} \right\}. \quad (S46)$$

With

$$\mu_\mathfrak{L}^{\sigma'} = E_\mathrm{F} + \frac{1}{2}eV + \frac{\hbar}{2}W_z^{(\mathfrak{L})}\sigma'$$

$$\mu_\mathfrak{R}^{\sigma'} = E_\mathrm{F} - \frac{1}{2}eV + \frac{\hbar}{2}W_z^{(\mathfrak{R})}\sigma'$$

[see also Eq. (S2)] we Taylor-expand the Fermi functions around equilibrium (at infinitesimal temperature) in order to obtain the current in linear response,

$$I = \frac{e}{h} \sum_m \sum_{\sigma'} \int \mathrm{d}E \left\{ n_\mathrm{F}(E - E_\mathrm{F}) \left[1 - \sum_\sigma R_{\sigma\sigma',m}^{(\mathfrak{L}\mathfrak{L})} - \sum_\sigma T_{\sigma\sigma',m}^{(\mathfrak{L}\mathfrak{R})} \right] + \right. \quad (S47)$$

$$+ \left[\frac{\partial n_\mathrm{F}(E - E_\mathrm{F})}{\partial E_\mathrm{F}} \right]_{E,T} \cdot \left[1 - \sum_\sigma R_{\sigma\sigma',m}^{(\mathfrak{L}\mathfrak{L})} + \sum_\sigma T_{\sigma\sigma',m}^{(\mathfrak{L}\mathfrak{R})} \right] \frac{eV}{2} + \quad (S48)$$

$$\left. + \frac{\hbar}{2}\sigma' \left[\frac{\partial n_\mathrm{F}(E - E_\mathrm{F})}{\partial E_\mathrm{F}} \right]_{E,T} \cdot \left[\left(1 - \sum_\sigma R_{\sigma\sigma',m}^{(\mathfrak{L}\mathfrak{L})} \right) W_z^{(\mathfrak{L})} - \sum_\sigma T_{\sigma\sigma',m}^{(\mathfrak{L}\mathfrak{R})} W_z^{(\mathfrak{R})} \right] \right\}. \quad (S49)$$

Expressing the reflection coefficients through transmissions by using unitarity, Eq. (S31), results in

- vanishing of the equilibrium term;

- furthermore, at zero temperature we get Landauer-Büttiker formula for the charge conductance, as given in the main text

- coefficients of the charge-current response to spin accumulations,

$$\tilde{G}_z^{(\mathfrak{L})} = +\frac{e}{4\pi} \sum_m \sum_{\sigma\sigma'} \sigma' T_{\sigma\sigma',m}^{(\mathfrak{R}\mathfrak{L})} \tag{S50a}$$

$$\tilde{G}_z^{(\mathfrak{R})} = -\frac{e}{4\pi} \sum_m \sum_{\sigma\sigma'} \sigma' T_{\sigma\sigma',m}^{(\mathfrak{L}\mathfrak{R})}. \tag{S50b}$$

In a similar way it is possible to derive expressions for the spin currents,

$$I_z^{(\mathfrak{L})} = \frac{1}{4\pi} \sum_m \sum_{\sigma'} \int dE (-1) \left\{ n_F(E - \mu_{\mathfrak{L}}^{\sigma'}) \sum_\sigma \sigma R_{\sigma\sigma',m}^{(\mathfrak{L}\mathfrak{L})} + n_F(E - \mu_{\mathfrak{R}}^{\sigma'}) \sum_\sigma \sigma T_{\sigma\sigma',m}^{(\mathfrak{L}\mathfrak{R})} \right\} \tag{S51}$$

$$I_z^{(\mathfrak{R})} = \frac{1}{4\pi} \sum_m \sum_{\sigma'} \int dE (+1) \left\{ n_F(E - \mu_{\mathfrak{R}}^{\sigma'}) \sum_\sigma \sigma R_{\sigma\sigma',m}^{(\mathfrak{R}\mathfrak{R})} + n_F(E - \mu_{\mathfrak{L}}^{\sigma'}) \sum_\sigma \sigma T_{\sigma\sigma',m}^{(\mathfrak{R}\mathfrak{L})} \right\}. \tag{S52}$$

Notice that the sign change from - to + is due to our definition of the positive direction of the current, see the definitions in the main text. The linearized expressions

$$
\begin{aligned}
I_z^{(\mathfrak{L})} = -\frac{1}{4\pi} \sum_m \sum_{\sigma'} \int dE \bigg\{ & n_F(E - E_F) \sum_\sigma \sigma \left[R_{\sigma\sigma',m}^{(\mathfrak{L}\mathfrak{L})} + T_{\sigma\sigma',m}^{(\mathfrak{L}\mathfrak{R})} \right] \\
& + \left(\frac{\partial n_F}{\partial E_F} \right) \frac{eV}{2} \sum_\sigma \sigma \left[R_{\sigma\sigma',m}^{(\mathfrak{L}\mathfrak{L})} - T_{\sigma\sigma',m}^{(\mathfrak{L}\mathfrak{R})} \right] + \\
& + \left(\frac{\partial n_F}{\partial E_F} \right) \frac{\hbar}{2} \sum_\sigma \sigma\sigma' \left[R_{\sigma\sigma',m}^{(\mathfrak{L}\mathfrak{L})} W_z^{(\mathfrak{L})} + T_{\sigma\sigma',m}^{(\mathfrak{L}\mathfrak{R})} W_z^{(\mathfrak{R})} \right] \bigg\},
\end{aligned}
$$

$$I_z^{(\mathfrak{R})} = +\frac{1}{4\pi}\sum_m\sum_{\sigma'}\int \mathrm{d}E\left\{n_\mathrm{F}(E-E_\mathrm{F})\sum_\sigma \sigma\left[R_{\sigma\sigma',m}^{(\mathfrak{R}\mathfrak{R})}+T_{\sigma\sigma',m}^{(\mathfrak{R}\mathfrak{L})}\right]\right.$$

$$+\left(\frac{\partial n_\mathrm{F}}{\partial E_\mathrm{F}}\right)\frac{eV}{2}\sum_\sigma \sigma\left[-R_{\sigma\sigma',m}^{(\mathfrak{R}\mathfrak{R})}+T_{\sigma\sigma',m}^{(\mathfrak{R}\mathfrak{L})}\right]+$$

$$\left.+\left(\frac{\partial n_\mathrm{F}}{\partial E_\mathrm{F}}\right)\frac{\hbar}{2}\sum_\sigma \sigma'\sigma\left[R_{\sigma\sigma',m}^{(\mathfrak{R}\mathfrak{R})})W_z^{(\mathfrak{R})}+T_{\sigma\sigma',m}^{(\mathfrak{R}\mathfrak{L})}W_z^{(\mathfrak{L})}\right]\right\}$$

deliver using Eq. (S32)

- vanishing equilibrium spin currents on accounts of unitarity,

- spin conductances as given in the main text, Eqs. (12b,d),

- response of the spin currents to spin accumulations characterised by coefficients:

$$G_{zz}^{(\mathfrak{L}\mathfrak{L})} = -\frac{\hbar}{8\pi}\sum_{\sigma\sigma'm}\sigma\sigma'\,R_{\sigma\sigma',m}^{(\mathfrak{L}\mathfrak{L})}$$

$$G_{zz}^{(\mathfrak{L}\mathfrak{R})} = -\frac{\hbar}{8\pi}\sum_{\sigma\sigma'm}\sigma\sigma'\,T_{\sigma\sigma',m}^{(\mathfrak{L}\mathfrak{R})}$$

$$G_{zz}^{(\mathfrak{R}\mathfrak{L})} = +\frac{\hbar}{8\pi}\sum_{\sigma\sigma'm}\sigma\sigma'\,T_{\sigma\sigma',m}^{(\mathfrak{R}\mathfrak{L})}$$

$$G_{zz}^{(\mathfrak{R}\mathfrak{R})} = +\frac{\hbar}{8\pi}\sum_{\sigma\sigma'm}\sigma\sigma'\,R_{\sigma\sigma',m}^{(\mathfrak{R}\mathfrak{R})}.$$

S5.2 Onsager's reciprocity relations

The reciprocity of spin conductances, $G_z^{(\mathfrak{L},\mathfrak{R})}$, and the coefficients, $\tilde{G}_z^{(\mathfrak{L},\mathfrak{R})}$, can be demonstrated readily. Upon employing the Eq. (S36c) in the formulæ Eq. (S50) and comparing with the Eqs. (12b,d) of the main text we readily confirm the reciprocal relations, Eqs. (S4a,S4b). In the same way the reciprocity (S4c) follows by employing time reversal symmetry of transmission probabilities.

S5.3   Nonzero spin conductance is due to spin-flip reflections

The spin conductances were defined in the main text. Using Eq. (S32) we can express them using reflection coefficients only. The spin-diagonal elements can be eliminated with the Eq. (S36a) and in time-reversal invariant situations only the spin-flipping processes contribute,

$$G_z^{(\mathfrak{R})} = \frac{e}{4\pi} \sum_m \left(R_{\downarrow\uparrow,m}^{(\mathfrak{R}\mathfrak{R})} - R_{\uparrow\downarrow,m}^{(\mathfrak{R}\mathfrak{R})} \right) \tag{S53a}$$

$$G_z^{(\mathfrak{L})} = \frac{e}{4\pi} \sum_m \left(R_{\downarrow\uparrow,m}^{(\mathfrak{L}\mathfrak{L})} - R_{\uparrow\downarrow,m}^{(\mathfrak{L}\mathfrak{L})} \right). \tag{S53b}$$

S5.4   A proof of $G_z^{(\mathfrak{R})} = -G_z^{(\mathfrak{L})}$

By adding the Eq. (S53) we obtain zero because of parity, Eq. (S44). It follows that

$$G_z^{(\mathfrak{R})} = -G_z^{(\mathfrak{L})}. \tag{S54}$$

Since the proof requires only basic symmetries, it is conceivable that the relation (S54) holds true for a wider class of Hamiltonians, the Eq. (S26) being an example. For instance, the contacts might be modeled by a smooth behavior of $\tilde{\kappa}(s)$ or the contacts might involve barrier tunneling. However, once the inversion symmetry is lost, *i.e.* when the coupling to the left lead is not the same as to the right, the identity Eq. (S54) ceases to hold.

It is also possible to derive the identity Eq. (S54) by using transmission probabilities only. To this end, we add the expressions

$$G_z^{(\mathfrak{R})} = \frac{e}{4\pi} \sum_m \left(T_{\uparrow\uparrow,m}^{(\mathfrak{R}\mathfrak{L})} + T_{\uparrow\downarrow,m}^{(\mathfrak{R}\mathfrak{L})} - T_{\downarrow\uparrow,m}^{(\mathfrak{R}\mathfrak{L})} - T_{\downarrow\downarrow,m}^{(\mathfrak{R}\mathfrak{L})} \right) \tag{S55a}$$

$$G_z^{(\mathfrak{L})} = \frac{e}{4\pi} \sum_m \left(T_{\uparrow\uparrow,m}^{(\mathfrak{L}\mathfrak{R})} + T_{\uparrow\downarrow,m}^{(\mathfrak{L}\mathfrak{R})} - T_{\downarrow\uparrow,m}^{(\mathfrak{L}\mathfrak{R})} - T_{\downarrow\downarrow,m}^{(\mathfrak{L}\mathfrak{R})} \right). \tag{S55b}$$

Discarding the constant prefactor we get an expression that can be regrouped into four rounded brackets,

$$\sum_m \left[\left(T_{\uparrow\uparrow,m}^{(\mathfrak{RL})} - T_{\downarrow\downarrow,m}^{(\mathfrak{LR})} \right) + \left(T_{\uparrow\uparrow,m}^{(\mathfrak{LR})} - T_{\downarrow\downarrow,m}^{(\mathfrak{RL})} \right) + \left(T_{\uparrow\downarrow,m}^{(\mathfrak{LR})} - T_{\downarrow\uparrow,m}^{(\mathfrak{RL})} \right) + \left(T_{\uparrow\downarrow,m}^{(\mathfrak{RL})} - T_{\downarrow\uparrow,m}^{(\mathfrak{LR})} \right) \right].$$

The first two brackets vanish on account of Eq. (S36c) and the remaining two because of Eq. (S44b).

S6   Spin and charge densities in the leads

Equilibrium spin and charge densities and their bias-induced counterparts are elaborated in this section from scattering wavefunctions. For the sake of specificity $m = \pm 1$.

S6.1   Local densities of scattering states

Wavefunctions in the left lead.   At a fixed energy $E = \frac{1}{2}q^2$ and m there are 4 scattering states, mapping asymptotically to spin up/down particles incoming from the left and right lead. In this section we label them L1, L2, R1 and R2. Their spinor wavefunctions were given in Sec. S3 and here we reproduce their expressions in the left lead ($s < 0$)

$$\psi_{L1,m}^{E}(s) = \frac{1}{\sqrt{2\pi}}\left[e^{iqs}\left|\uparrow\right\rangle + e^{-iqs}\sum_{\sigma} r_{\sigma\uparrow,m}^{(\mathcal{LL})}\left|\sigma\right\rangle\right] \tag{S56a}$$

$$\psi_{L2,m}^{E}(s) = \frac{1}{\sqrt{2\pi}}\left[e^{iqs}\left|\downarrow\right\rangle + e^{-iqs}\sum_{\sigma} r_{\sigma\downarrow,m}^{(\mathcal{LL})}\left|\sigma\right\rangle\right] \tag{S56b}$$

$$\psi_{R1,m}^{E}(s) = \frac{1}{\sqrt{2\pi}}e^{-iqs}\sum_{\sigma} t_{\sigma\uparrow,m}^{(\mathcal{LR})}\left|\sigma\right\rangle \tag{S56c}$$

$$\psi_{R2,m}^{E}(s) = \frac{1}{\sqrt{2\pi}}e^{-iqs}\sum_{\sigma} t_{\sigma\downarrow,m}^{(\mathcal{LR})}\left|\sigma\right\rangle . \tag{S56d}$$

Notice that we employ a plane-wave normalization factor $1/\sqrt{2\pi}$, unlike in Sec. S3.

Direction-resolved densities.   In equilibrium, spin and charge densities can be obtained straightforwardly by calculating the local density of states from the above wavefunctions. In bias-induced stationary nonequilibrium we need to discriminate between states incoming from left and right.

For given $q > 0$ and $s < 0$, the spin- and direction-resolved densities from the states (S56)

read

$$n_{\uparrow,L}(q,s) = \frac{1}{2\pi} \sum_m \left\{ 1 + 2\,\mathrm{Re}\left[e^{-\mathrm{i}2qs} r_{\uparrow\uparrow,m}^{(\mathcal{LL})} \right] + R_{\uparrow\downarrow,m}^{(\mathcal{LL})} + R_{\uparrow\uparrow,m}^{(\mathcal{LL})} \right\},$$

$$n_{\downarrow,L}(q,s) = \frac{1}{2\pi} \sum_m \left\{ 1 + 2\,\mathrm{Re}\left[e^{-\mathrm{i}2qs} r_{\downarrow\downarrow,m}^{(\mathcal{LL})} \right] + R_{\downarrow\downarrow,m}^{(\mathcal{LL})} + R_{\downarrow\uparrow,m}^{(\mathcal{LL})} \right\},$$

$$n_{\uparrow,R}(q,s) = \frac{1}{2\pi} \sum_m \left\{ T_{\uparrow\downarrow,m}^{(\mathcal{LR})} + T_{\uparrow\uparrow,m}^{(\mathcal{LR})} \right\},$$

$$n_{\downarrow,R}(q,s) = \frac{1}{2\pi} \sum_m \left\{ T_{\downarrow\downarrow,m}^{(\mathcal{LR})} + T_{\downarrow\uparrow,m}^{(\mathcal{LR})} \right\}.$$

Spin and charge densities at energy $E = \frac{1}{2}q^2$. The (dimensionless) charge and spin densities follow directly from the above relations by summing the L and R contributions equally. First, the charge density at $s < 0$ reads

$$n_0(q,s) = \sum_\sigma \left[n_{\sigma,L}(q,s) + n_{\sigma,R}(q,s) \right] = \frac{1}{\pi} \sum_m \mathrm{Re} \left\{ 2 + e^{-\mathrm{i}2qs} \left(r_{\uparrow\uparrow,m}^{(\mathcal{LL})} + r_{\downarrow\downarrow,m}^{(\mathcal{LL})} \right) \right\}, \qquad \text{(S57)}$$

where Eq. (S31) was applied. Note that the charge density from eigenstates at energy E in a clean infinite tube is $8/2\pi$ (due to twofold spin, orbital and direction degeneracies), which is just the first term in the above expression. The oscillating term occurs because (only) the spin-diagonal reflection amplitudes lead to a *coherent* sum of two planewaves with opposite momenta. Spin-flipping processes contribute incoherently, because the incident and reflected waves pertain to disjoint Hilbert subspaces due to the opposite spins of the waves.

Second, the spin density vanishes on accounts of time-reversal invariance (TRI), Eq. (S36a).

$$n_z(q,s) = \sum_\sigma \sigma[n_{\sigma,L}(q,s) + n_{\sigma,R}(q,s)] = \frac{1}{\pi} \sum_m \mathrm{Re} \left\{ e^{-\mathrm{i}2qs} \left(r_{\uparrow\uparrow,m}^{(\mathcal{LL})} - r_{\downarrow\downarrow,m}^{(\mathcal{LL})} \right) \right\} \overset{\text{(TRI)}}{=} 0. \quad \text{(S58)}$$

Spin and charge densities at energy E for nonequilibrium. At a finite bias voltage, the symmetry between L and R states is broken. The charge density is determined by the difference between L and R densities provided that the bias difference V applies symmetrically

on both leads. In such cases, the difference reads

$$\sum_\sigma \left[n_{\sigma,L}(q,s) - n_{\sigma,R}(q,s) \right] =$$

$$= \frac{1}{2\pi} \sum_m \left\{ 2 + 2\,\mathrm{Re} \left[e^{-\mathrm{i}2qs} \left(r_{\uparrow\uparrow,m}^{(\mathcal{LL})} + r_{\downarrow\downarrow,m}^{(\mathcal{LL})} \right) \right] + \sum_{\sigma\sigma'} \left(R_{\sigma\sigma',m}^{(\mathcal{LL})} - T_{\sigma\sigma',m}^{(\mathcal{LR})} \right) \right\}. \quad \text{(S59)}$$

The terms above have a rather transparent meaning. Employing the Eq. (S31) to convert the reflection probabilities into transmission and recognizing the linear conductance formula, the previous expression simplifies to

$$\frac{1}{\pi} \sum_m \left\{ 2 + \mathrm{Re} \left[e^{-\mathrm{i}2qs} \left(r_{\uparrow\uparrow,m}^{(\mathcal{LL})} + r_{\downarrow\downarrow,m}^{(\mathcal{LL})} \right) \right] - \sum_{\sigma\sigma'} T_{\sigma\sigma',m}^{(\mathcal{LR})} \right\}$$

$$\text{(TRI)} \quad = \frac{1}{\pi} \left(4 - \frac{h}{e^2} G \right) + \frac{2}{\pi} \sum_m \mathrm{Re} \left[e^{-\mathrm{i}2qs} r_{\uparrow\uparrow,m}^{(\mathcal{LL})} \right]. \quad \text{(S60)}$$

The application of TRI in the last line is indicated. The expression (S60) offers an interpretation: The total number of L fluxes is 4. To this number, an effective count of backreflected states, $-hG/e^2$, and an interference term are to be added.

Analogously for the spin density in the left lead,

$$\sum_\sigma \sigma \left[n_{\sigma,L}(q,s) - n_{\sigma,R}(q,s) \right] =$$

$$= \frac{1}{\pi} \sum_m \left\{ \mathrm{Re} \left[e^{-\mathrm{i}2qs} \left(r_{\uparrow\uparrow,m}^{(\mathcal{LL})} - r_{\downarrow\downarrow,m}^{(\mathcal{LL})} \right) \right] + \sum_{\sigma\sigma'} \sigma \left(R_{\sigma\sigma',m}^{(\mathcal{LL})} - T_{\sigma\sigma',m}^{(\mathcal{LR})} \right) \right\}.$$

Unitarity, TRI and the definition of spin conductance simplify the expression,

$$\sum_\sigma \left[n_{\sigma,L}(q,s) - n_{\sigma,R}(q,s) \right] = -\frac{1}{\pi} \sum_m \sum_{\sigma\sigma'} \sigma T_{\sigma\sigma',m}^{(\mathcal{LR})}$$

$$= -\frac{1}{\pi} \frac{4\pi}{e} G_z^{(\mathcal{L})} \Bigg|_{E=q^2/2}. \quad \text{(S61)}$$

S6.2   Surface- and bulk-accumulated densities

In order to get energy-unresolved equilibrium and non-equilibrium charge and spin densities (accumulations), the formulæ (S61,S60,S57) have to be integrated over an energy window.

Equilibrium densities.   The integration of the Eq. (S57) delivers a homogeneous term and a term that oscillates,

$$n_0(s)\Big|_{V=0} = n_\infty + \frac{2}{\pi} \sum_m \int_0^{q_F} \frac{dq}{2\pi} \, \mathrm{Re}\left[e^{-i2qs} \, r_{\uparrow\uparrow,m}^{(\mathcal{LL})}\right], \quad q_F = \sqrt{2E_F}, \; s < 0.$$

with $n_\infty = 2q_F/\pi^2$ being the Fermi ground-state density of a transparent infinite four-channel conductor. The oscillating term describes familiar Friedel oscillations that decay asymptotically as $1/q_F s$ from the contact into the bulk. The equilibrium charge density therefore has a bulk term and a *surface accumulation.*

The spin density in equilibrium is zero because of TRI.

Nonequilibrium densities induced by a voltage bias.   These observables are given by summing the density of L states with energies $E \in \langle E_F, E_F + V/2 \rangle$ and subtracting the contribution of R states in $\langle E_F - V/2, E_F \rangle$. We achieve this readily by integrating the Eq. (S60) in $q \in \langle q_F, \sqrt{2(E_F + V/2)} \rangle$. In first order in V the charge density for $s < 0$ reads

$$\delta n_0(s) = \int_{q_F}^{q_F + V/2q_F} \frac{dq}{2\pi} \left\{ \frac{1}{\pi}\left(4 - \frac{h}{e^2}G\right) + \frac{2}{\pi}\sum_m \mathrm{Re}\left[e^{-i2qs} \, r_{\uparrow\uparrow,m}^{(\mathcal{LL})}\right] \right\} \qquad + \mathcal{O}(V^2)$$

$$= V \, \varrho_L(E_F)\left[\left(4 - \frac{h}{e^2}G\right) + 2\sum_m \mathrm{Re}\left\{e^{-i2qs} r_{\uparrow\uparrow,m}^{(\mathcal{LL})}\right\}\right] \qquad + \mathcal{O}(V^2),$$

where we introduced the local density of left-moving states in a single channel (spinless) transparent wire

$$\varrho_L(E_F) = \frac{1}{4\pi^2 q_F} = \frac{1}{8}\frac{\partial n_\infty}{\partial E}\Big|_{E=E_F}. \tag{S62}$$

The bulk term $V\varrho_L(E_F)\left(4 - \frac{h}{e^2}G\right)$ vanishes in the transparency limit. The oscillating term

is straightforwardly connected to the equilibrium Friedel oscillations.

The spin-density is nonzero because the voltage breaks symmetry between the L and R states; from the Eq. (S61) we get

$$\delta n_z(s) = -V \, \varrho_L(E_F) \frac{4\pi}{e} G_z^{(\mathfrak{L})} + \mathcal{O}(V^2), \quad s < 0. \tag{S63}$$

The voltage-induced spin density does not have a surface component, only a bulk one.

Spin accumulation. The homogeneous voltage-induced spin density offers a simple estimate for the spin accumulation, *i.e.* the spin-polarized chemical potential (see Eq. (S2)), in linear response to V. Namely,

$$\hbar W_z^{(\mathfrak{L})}(V) = \mu_\uparrow^{(\mathfrak{L})}(V) - \mu_\downarrow^{(\mathfrak{L})}(V) \approx \left. \frac{\partial E_F}{\partial n} \right|_{n=n_\infty} \delta n_z(s) \tag{S64}$$

$$= -V \frac{\pi}{2e} G_z^{(\mathfrak{L})}, \tag{S65}$$

where we used (S63,S62).

The expression holds true only if one can neglect spin scattering at the interface between the lead (tube) and the contacts of the battery.

References

(1) Kiselev, A.; Kim, K. Prohibition of equilibrium spin currents in multiterminal ballistic devices. Phys. Rev. B **2005**, 71, 153315.

(2) Onsager, L. Reciprocal Relations in Irreversible Processes. II. Phys. Rev. **1931**, 38, 2265–2279.

(3) Casimir, H. B. G. On Onsager's Principle of Microscopic Reversibility. Rev. Mod. Phys. **1945**, 17, 343–350.

(4) Nazarov, Y. V.; Blanter, Y. M. Quantum Transport: Introduction to Nanoscience; Cambridge University Press, 2009.

(5) Yang, X.; van der Wal, C. H.; van Wees, B. J. Spin-dependent electron transmission model for chiral molecules in mesoscopic devices. Phys. Rev. B **2019**, 99, 024418.

(6) Jacquod, P.; Whitney, R. S.; Meair, J.; Büttiker, M. Onsager relations in coupled electric, thermoelectric, and spin transport: The tenfold way. Phys. Rev. B **2012**, 86, 155118.

(7) Sánchez, D.; Serra, L. m. c.; Choi, M.-S. Strongly modulated transmission of a spin-split quantum wire with local Rashba interaction. Phys. Rev. B **2008**, 77, 035315.